8-1-2019 1:00 PM

Neurodevelopmental Outcomes of Infantile Hydrocephalus: An fMRI Case Study

Ikhlas Ahmed Hashi, *The University of Western Ontario*

Supervisor: Sandrine de Ribaupierre, *The University of Western Ontario*

A thesis submitted in partial fulfillment of the requirements for the Master of Science degree in Neuroscience

Abstract

Ventricle dilatation caused by infantile hydrocephalus may result in extensive damage of the posterior cortex (parietal and occipital lobes). We hypothesize that pathological changes in the development of the posterior cortex can be linked to non-verbal learning disabilities in children with previous infantile hydrocephalus. This case study will investigate the neurodevelopmental outcomes of 3 treated hydrocephalus patients, when compared to a group of healthy control children (n = 12). Within the hydrocephalus group, patients displayed differences in non-verbal test performance as well as parietal brain activation during an fMRI number comparison task. We associated these differences with clinical variables such as prematurity of birth, age of onset, and timing of treatment. The methodology and findings of this case study offers new possibilities for future research of using fMRI in conjunction with behavioural assessments as a prognostic tool for studying the neurodevelopmental outcomes of pediatric patient populations.

Keywords

infantile hydrocephalus, functional Magnetic Resonance Imaging (fMRI), blood-oxygen-level dependent (BOLD) signal, pediatrics, non-verbal learning, ventricle dilatation, posterior cortex, developmental neuroscience.

Summary for Lay Audience

Infantile hydrocephalus is a medical condition which involves the inadequate drainage of cerebrospinal fluid (CSF), a clear fluid that circulates within the brain and spinal cord and can occur during the first two years of life. There can be multiple causes of infantile hydrocephalus, such as genetic malformations, premature birth that may lead to bleeding in the brain, and severe bacterial infections of the brain such as meningitis. The buildup of CSF within the skull, can result in an increase in pressure and damage to surrounding brain areas. The compression of the developing brain may lead to negative outcomes in behavior and cognition, as well as the emergence of various developmental disabilities during childhood. Due to the progression pattern of hydrocephalus, areas of the brain located towards the back (posterior brain areas) will experience greater damage and compression when compared to brain areas towards the front (anterior brain areas). This current study will examine whether changes in development of the posterior brain will lead to deficits in non-verbal learning, their associated cognitive outputs. Non-verbal learning includes mathematics, visual processing, and spatial orientation skills. The current study involves the cases of 3 treated hydrocephalus patients and a group of healthy control children to assess and compare their behavioural outcomes. Functional MRI (fMRI) was used to measure brain activity in parietal cortex during a number comparison task, children played during the MRI scan. Differences in the behavioural test scores and brain activity were found among the patients, we associated these differences to various clinical and socioeconomic variables. The experimental design and findings of this study offer new avenues for future research into using fMRI with behavioural tests as a tool for studying the developmental outcomes for pediatric patient populations such as hydrocephalus.

Co-Authorship Statement

This thesis contains material from a manuscript, titled *Nonverbal Learning Outcomes in Infantile Hydrocephalus Patients: An fMRI Case Study,* that is in preparation for publication in the journal *Clinical Neurology and Neurosurgery*. The manuscript was co-authored by Ikhlas Hashi, Dr. Sandrine de Ribaupierre, Dr. Roy Eagleson and Estelle Ansermet. Ikhlas Hashi made contributions to all aspects of the study by helping design the experimental protocol, enrolled participants, ran behavioural assessments and MRI scans to acquire data. In addition, Ikhlas, also analyzed all of the collected data and drafted the manuscript. All work was conducted under the supervision and support of Dr. de Ribaupierre. Dr. de Ribaupierre formulated the initial research question and experimental protocol. Dr de Ribaupierre also help with analyzing data and editing the manuscript. Dr. Eagleson provided guidance with analyzing and interpreting the data. Estelle Ansermet helped design the experimental protocol and conduct the behavioural assessments.

Acknowledgments

I would like to sincerely thank my supervisor, Dr. Sandrine de Ribaupierre, for her support and guidance. Thank you for taking me on as your master's student. Thank you for your mentorship and providing me with the essential tools for my project to grow. I would also like to thank all of my academic advisors. Dr. Roy Eagleson and Dr. J. Bruce Morton thank you for insights, advice, your feedback during my advisory committee and lab meetings. Dr. Derek Mitchell, thank you for your guidance, feedback, and direction throughout the course of my master's. I would like to especially thank Dr. Daniel Ansari, for your support these past two years, whether that would be by providing me with essential feedback during my advisory committee meetings, setting up fMRI tasks, helping me with data analysis, or reviewing my thesis. Your intellectual insight, expertise, and work ethic is truly inspiring. I am grateful for your mentorship.

In addition, I would like to thank Ms. Bea Goffin, for her help with recruitment, providing me with behavioural tests, and teaching me about the mock scan. I would also like to thank the Centre for Functional and Metabolic Mapping staff, for helping me run the MRI scans. I would like to especially thank Mr. Scott Charlton, for helping ensure the MRI protocol ran so smoothly, and making scans enjoyable and fun for our young participants and their families.

To the Brain3dViz lab members thank you for your support throughout the course of my master's. I would like to especially thank Estelle Ansermet, for all your help with setting up my project, and teaching me how to run the behavioural tests. Thank you, Marcus Lo, for helping me recruit patients, collecting clinical data, and being the first participant during our pilot MRI scan. I would also like to thank my fellow trainees Daamoon Ghahari and Daiana Pur for all of their support and help.

I would like to thank my parents and siblings for their unwavering support, boundless motivation and endless encouragement. A special thanks to all my participants and their families for their consent and participation, whom without this project would have not been possible. Finally, I would like to thank our funding sources: BrainsCAN and Children's Health Research Institute, for making this project possible.

Table of Contents

List of Tables

List of Figures

List of Abbreviations

CSF – cerebrospinal fluid

CNS – central nervous system

IVH – intraventricular hemorrhage

ICP – intracranial pressure

VD – ventricle dilatation

US – ultrasound

CT – computerized tomographic scan

MRI – magnetic resonance imaging

NICU - neonatal intensive care unit

fMRI – functional magnetic resonance imaging

BOLD – Blood-oxygen-level dependent

ROI – region of interest

SES – socioeconomic status

mg/dl – milligrams per decilitre

VP – ventriculoperitoneal

ETV – endoscopic third ventriculostomy

g – grams

ROI – region of interest

T – tesla

CFMM - Centre of Functional and Metabolic Mapping

ep – echo planar

TE – echo time

TR – repetition time

FOV – field of view

mm – milometers

Beery VMI – Beery-Buktenica Developmental Test of Visual Motor Integration

VMI – Visual Motor Integration

NSS – Number Sense Screener

WPPSI – Wechsler Preschool and Primary Scale of Intelligence

WISC – Wechsler Intelligence Scale for Children

DICOM – Digital Imaging and Communications in Medicine

NIfTI – Neuroimaging Informatics Technology Initiative

BIDS – Brain Imaging Data Structure

FSL - FMRIB Software Library

BET – Brain Extraction Tool

FEAT – FMRIB's Easy Analysis Tool

FWHM – full-width at half maximum

BBR – boundary-based registration

DOF – degrees of freedom

MNI – Montreal Neurological Institute

NIH – National Institute of Health

NIHPD – MRI Study of Normal Brain Development

GLM – general linear model

EVs – explanatory variables

COPE – combination of parameter estimates

FWE – family wise error rate

IPS – intraparietal sulcus

SPL – superior parietal lobule

List of Appendices

Chapter 1

1 Introduction

1.1 Infantile Hydrocephalus

Derived from the ancient Greek word ‘hudrokephalon’ which literally translates to ‘water’ ‘head’, hydrocephalus is the accumulation of excess fluid in the brain (Aschoff et al., 1999; hydrocephalus | Definition of hydrocephalus in English by Oxford Dictionaries; Rekate, 2008). The International Working Group Hydrocephalus defines hydrocephalus as a neurological condition which involves the progressive distension of the brain’s ventricular system due to the over production or obstruction of the flow of the cerebrospinal fluid (CSF) between its site of production in the ventricular system and its point of absorption, in the subarachnoid space surrounding the brain (Hydrocephalus During Infancy | The Embryo Project Encyclopedia). Infantile Hydrocephalus is a form of hydrocephalus which develops in children within the first two years of life (Tully and Dobyns, 2014) (Figure 1). Hydrocephalus is the most common disease treated by pediatric neurosurgeons (Kahle et al., 2016).

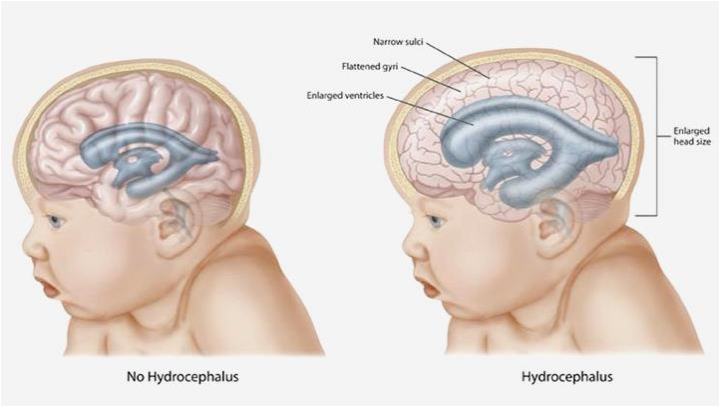

Figure 1: A common feature of infantile hydrocephalus is a large head circumference which can be accredited to an increase in intraventricular pressure leading to ventricular dilatation (VD) and consequently an increase in head circumference (From: Hydrocephalus, 2019).

CSF has multiple functions in maintaining the homeostasis of the brain and providing mechanical protection to the brain by working as a fluid cushion (Cinalli et al., 2004; McAllister et al., 1991b) . There are four cerebral ventricles which consist of: the two lateral ventricles, third ventricle and fourth ventricle. A disruption in the flow of CSF (or an overproduction of CSF) can result in the accumulation of CSF in the ventricles, causing the ventricles to expand through ventricular dilatation and the development of hydrocephalus (Cinalli et al., 2004; Raybaud, 2017). The normal flow of CSF is illustrated in Figure 2.

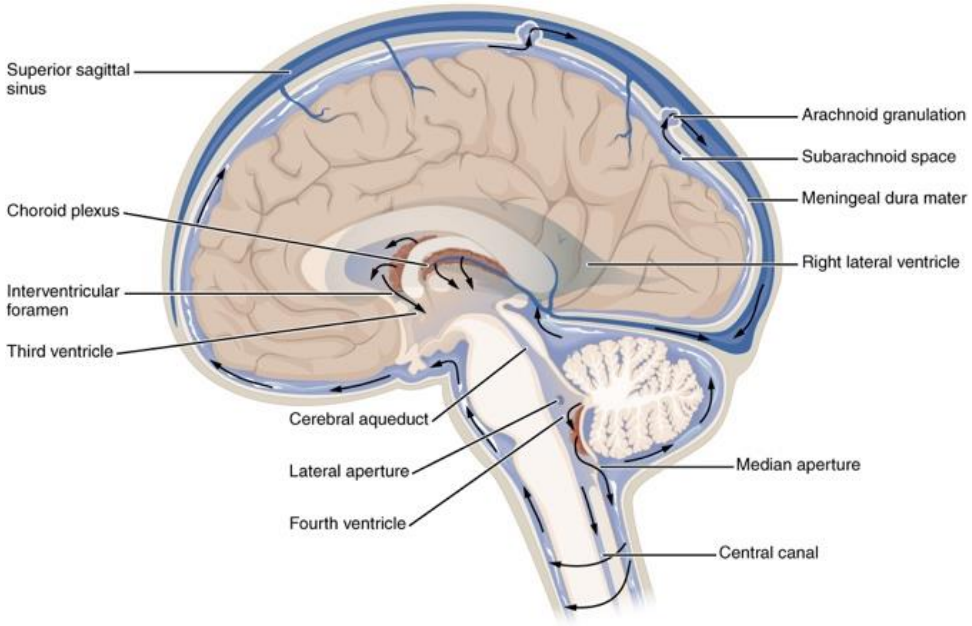

Figure 2: Flow of CSF begins in the lateral ventricles then to the third ventricle via the foramen of Monro, after which CSF passes through the cerebral aqueduct into the fourth ventricle and leaving through the foramina of Luschka and Magendie (From: Cerebrospinal fluid, 2019; Wright et al., 2016), where it enters the subarachnoid space, circulating around brain and spinal cord until it finally reaches the arachnoid granulations, into venous circulation (From: Cerebrospinal fluid, 2019).

The classification of infantile hydrocephalus depends site of CSF obstruction, the cause of the obstruction as well as the age of onset. In communicating hydrocephalus, there is no blockage in the flow of CSF in the ventricle system but rather CSF build-up arises from insufficient absorption (in the case of infection such as meningitis or hemorrhage) or CSF overproduction (Wright et al., 2016). In contrast, noncommunicating or obstructive hydrocephalus occurs due to

an obstruction in the flow of CSF in the cerebral ventricles (Wright et al., 2016). Depending on the age of onset, infantile hydrocephalus can be defined as either being congenital or acquired. Congenital hydrocephalus is present at the time of birth, and may come as result of maternal infection, birth defects such as spina bifida, cerebral ventricle bleeding (intraventricular hemorrhage), or due to genetic mutations (Dandy Walker cysts, X-linked hydrocephalus) (Tully and Dobyns, 2014; Wright et al., 2016). Acquired hydrocephalus occurs after birth, due to infections, tumors, or genetic disorders (Tully and Dobyns, 2014; Wright et al., 2016). Intraventricular hemorrhage (IVH) is the most common cause of hydrocephalus for newborns (Tully and Dobyns, 2014). Note that intraventricular hemorrhage may be classified as both acquired and congenital. The greatest risk factors for neonatal IVH is prematurity coupled with a low birth weight of less than 1500 grams (Adams-Chapman et al., 2008). Prematurity is defined as infants who are born before 37 weeks. Most full-term infants are born with an approximate gestational age of 40 weeks and an average birth weight of 3500g (range of 2500 – 4500g) (Physical Growth in Newborns - Topic Overview). By classifying the type and underlying cause of infantile hydrocephalus, physicians can navigate the most appropriate treatment options to stabilize and manage patients.

1.2 Clinical Presentation and Symptoms

The severity of symptoms associate with infantile hydrocephalus can vary, mainly depending on the age of onset and the underlying cause of infantile hydrocephalus. Generally most of the signs and symptoms of hydrocephalus result from the increase in intracranial pressure (ICP) and ventricular dilatation (Wright et al., 2016). Neonates with hydrocephalus can present with the Cushing triad, a physiological response that consists of increased blood pressure, decreased heart rate and decrease respiration (Del Bigio, 1993; McAllister et al., 1991a; Wright et al., 2016). Older infants may display behavioural changes such as irritability, high pitch crying, and lethargy, as well as weight loss and vomiting (Hydrocephalus During Infancy | The Embryo Project Encyclopedia).

Macrocephaly (large head circumference) is by far the most identifiable symptom associated with infantile hydrocephalus. Macrocephaly can be accredited to the late closure of the cranial

bones in the skull, that are replaced with soft membranous gaps known as fontanelle (Del Bigio, 1993; Kahle et al., 2016; Tully and Dobyns, 2014; Wright et al., 2016). ICP causes the fontanelle to push outwards, increasing head circumference of the infant and thus developing macrocephaly. As the head circumference increases, the infant's fontanelle may bulge forward causing them to appear to be constantly looking downwards, developing "sunset eyes" (Bigio, 2010; Del Bigio, 1993). The veins of scalp veins dilate and become more prominent as head size increase. Continual head measurements are required in order to monitor further head growth and treat hydrocephalus.

1.3 Monitoring

Physicians and healthcare providers may use multiple neuroimaging techniques to non-invasively monitor the neuroanatomical changes associated with infantile hydrocephalus. At present, the most common imaging techniques being used are cranial ultrasound (US), computerized tomographic (CT) scan, and magnetic resonance imaging (MRI). In infants whose fontanelles have not yet been closed, cranial US, Figure 3, can measure ventricle size and detect the presence of lesions, hemorrhage, as well as periventricular cysts (Brouwer et al., 2010; Halm et al., 2018; Kishimoto et al., 2018; Obeid et al., 2019; Raybaud, 2017). The periventricular white matter adjacent to the lateral ventricles are highly susceptible to injury, which can be characterized by the presence of fluid filled cysts, known as periventricular cysts, shown in figure 3B. Due its limitations of having low resolution, cranial US cannot distinguish between the third and fourth ventricles, thereby hindering it from determining the underlying etiology of forms of infantile hydrocephalus which involve CSF obstruction in these areas (Wright et al., 2016).

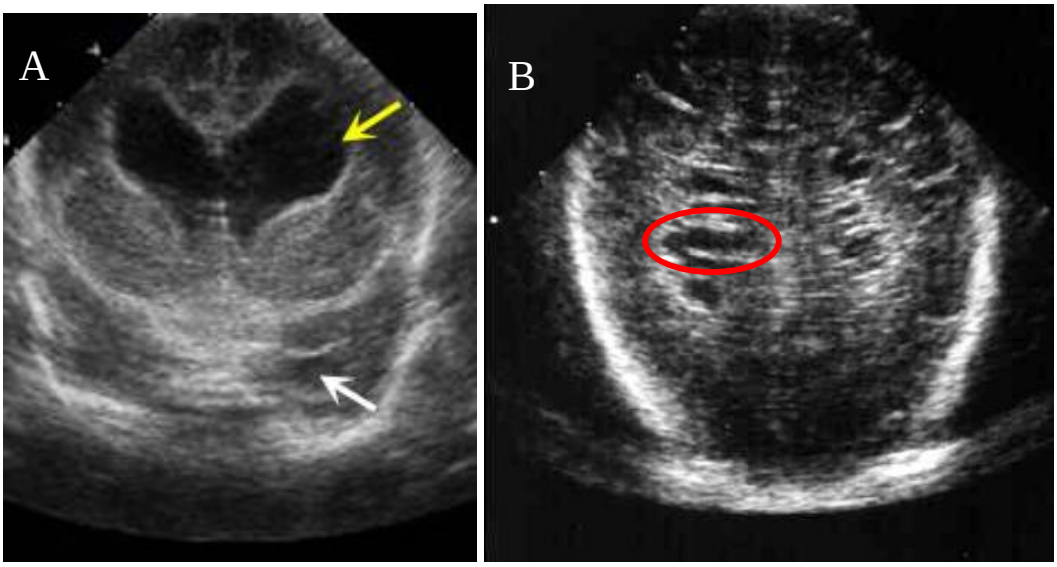

Figure 3: (A) The cranial US of an infant with hydrocephalus. Note the dilatation of lateral ventricles' frontal horns, indicated by the yellow arrow, and temporal horn, indicated by the white arrow(From: Hydrocephalus, 2019). (B) The US of a premature infant with marked periventricular cysts, circled in red (From: Pediatric Radiology).

CT scans are an efficient method of imaging that can display ventricle dilatation, lesions, tumors, and hemorrhage (Raybaud, 2017; Wright et al., 2016). Moreover, CT scans can be used to identify ICP by observing neuroanatomical changes such as: edema and decrease subarachnoid space (Raybaud, 2017; Wright et al., 2016). However, due to radiation exposure that is associated with CT scans, it is generally recommended in emergency situations only (Wright et al., 2016). There is an increasing shift towards using MRI (

Figure 4) for monitoring hydrocephalus. Primarily due to the fact that MRI scans are free of radiation exposure and provide greater anatomical precision over CT scans, making MRI a far more useful method of imaging that enable more accurate diagnosis and better management for treating hydrocephalus. MRI scans uses magnetic fields to scan the brain and create an anatomical image (Principles of magnetic resonance imaging - 1, 2015). Different techniques of MRI have emerged such as phase-contrast cine MRI and fast-sequence MRI. Phase-contrast cine MRI can be used to examine CSF flow and point of obstruction (Battal et al., 2011). Fast-

sequence MRI requires no patient sedation and is extremely efficient in acquiring images (Patel et al., 2014)

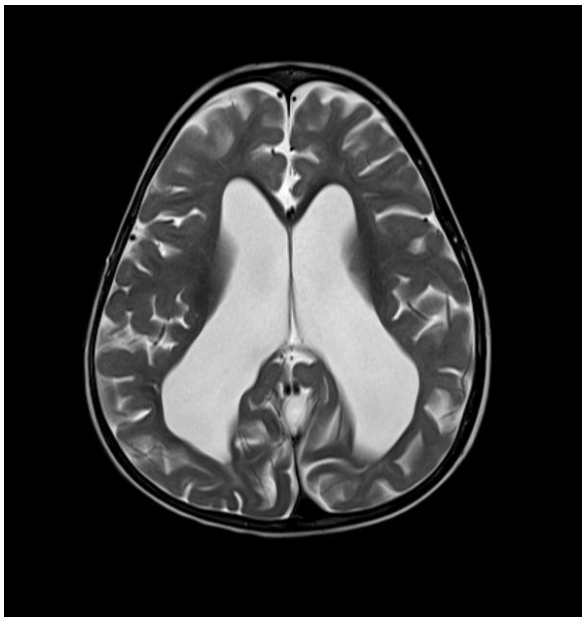

Figure 4: T2-weighted MRI image of a two-year-old male hydrocephalus patient with Dandy-Walker syndrome. (DWS) (From: Gaillard)

1.4 Treatment

The goals of treating infantile hydrocephalus is to reduce intracranial pressure and the extent of ventricular dilatation by draining excess CSF in order to diminish the risk of obtaining further damage of surrounding brain areas. Very young preterm infants often undergo temporizing treatments methods that require frequent surgical intervention and medical observations at the neonatal intensive care unit (NICU). Before proceeding to more permanent forms of treatment, such as shunts, various criteria must be met. For instance, the infant must weigh at least 1000 g and have a CSF protein level of around 1000 mg/dl (Fulmer et al., 2000). Common temporizing treatments include ventricular taps, Ommaya reservoirs, and ventriculosubgaleal shunts. Ommaya reservoirs involve placing a small device, or reservoir, that collects CSF beneath the scalp. Through ventricle tapping, a neurosurgeon can insert a syringe directly into the reservoir to remove the collected CSF (Krause et al., 2017, 2018; Lin et al., 2009). Ventriculosubgaleal shunts are a another temporary from of treatment, which involves inserting a catheter into the lateral ventricles, in order to shunt CSF into subgaleal space of the brain (Fulmer et al., 2000).

Older infants with continual head growth and worsened symptoms, permanent forms of treatment should be considered. Permanent treatments for hydrocephalus most often involve CSF diversion which allows for the continual drainage of CSF by diverting its flow to another area in the body via an alternative route (McAllister et al., 1991a; Pan, 2018; Wright et al., 2016). The most common form of CSF diversion is the ventriculoperitoneal (VP) shunt and endoscopic third ventriculostomy (ETV) (Agarwal et al., 2017; Rubin et al., 2008; Wright et al., 2016). VP shunts can be inserted into one of the cerebral ventricles, usually the lateral ventricles. The VP shunt can then extract CSF and divert it, via a long catheter, to the peritoneal space of the stomach, where CSF can be drained, Figure 5 (Tully and Dobyns, 2014; Wright et al., 2016).

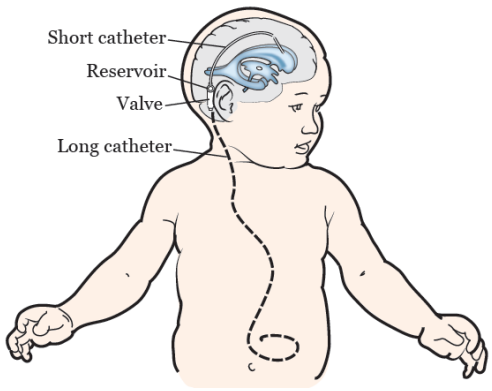

Figure 5: The ventriculoperitoneal (VP) shunt, shown in the above figure (From: About Your Ventriculoperitoneal (VP) Shunt Surgery for Pediatric Patients), is the most common form of ventricular shunts for infantile hydrocephalus treatment (From: Wright et al., 2016).

The endoscopic third ventriculostomy (ETV) can be used to treat non-communicating hydrocephalus (Cavalheiro et al., 2017; Krause et al., 2017, 2018; Wright et al., 2016; Yadav et al., 2012). Ventriculostomy is a surgical procedure which involves creating a small hole in the third ventricle. Once the hole is created CSF can bypass the obstructed ventricles and directly enter the subarachnoid space (Cavalheiro et al., 2017; Yadav et al., 2012). Ventriculostomies have been used treat hydrocephalus since as early as 1922, and only decreased in popularity during the advent of the shunts in 1960s (Aschoff et al., 1999). The renewal of ventriculostomy

has come as a result of the development of neuroendoscopy (endoscopy) (Cavalheiro et al., 2017; Di Rocco et al., 2006; Rekate, 2008; Wright et al., 2016; Yadav et al., 2012). During neuroendoscopy, a small camera is inserted into the third ventricle allowing neurosurgeons to view the ventricular system while performing the ventriculostomy.

1.5 Neuroanatomical Changes in the Posterior Cortex

Medical imaging tools such as fast sequence MRI, and treatment methods such as the VP shunt and ETV have significantly improved the prognosis of infantile hydrocephalus (Bigio, 2010). Despite these advancements infantile hydrocephalus is not free from complications. Neuroimaging studies involving the pathogenesis of hydrocephalus have observed progressive pathological changes in neuroanatomy due to increased intracranial pressure and ventricle dilatation. The extent of injury to surrounding brain areas primarily depends on the patient's age at the time of onset. The age of the patient is especially important when considering the stage of neuroanatomical development. Furthermore the rate of progression ventricle expansion, and how close the cortical lobe is to the ventricles is also important (Bigio, 2010; Dennis et al., 1981a; Dorner et al., 2018; Holwerda et al., 2016). The neurodevelopmental deficits in which patients with hydrocephalus may experience primarily depend upon which brain areas are affected during the pathogenesis of the condition. Studies investigating the neuroanatomical changes associated with infantile hydrocephalus using diffusion tension imaging (DTI), a neuroimaging technique used to measure white matter integrity; have found regional network abnormalities in cortical areas such as: the superior parietal, cingulate gyrus, medial frontal gyrus, and medial occipital gyrus (Kulkarni et al., 2015; Yuan et al., 2015, 2016). Brain abnormalities such as these have been associated to a range of developmental disabilities in: visuospatial skills, motor processing, memory, and executive function (Bigio, 2010; Brouwer et al., 2012; Del Bigio, 1993; Dennis et al., 1981a; Fletcher et al., 1992; Kulkarni et al., 2011; Lindquist et al., 2008; Mataró et al., 2001; Yeates et al., 2003; Yuan et al., 2016). Furthermore, hydrocephalic children were also recorded to have lower IQ scores and poor academic performance when compared to healthy controls (Mataró et al., 2001; Zahl et al., 2019).

An area of the brain that has been emphasized a great deal when studying pathological anatomical changes associated with infantile hydrocephalus is the posterior cortex which is defined as the parietal and occipital lobes. The posterior cortex has been cited by various studies

to undergo proportionally greater damage than anterior brain areas (Brouwer et al., 2010, 2016; Dorner et al., 2018; Fletcher et al., 1996b; Gammal et al., 1987; McAllister et al., 1991a). Neuropathological changes of the posterior cortex can be accredited to a multitude of factors. Such as, the direction of ventricular dilatation, which progresses posterior to anterior, causing the posterior cortex to undergo prolonged compression, increased inflammation, pronounced cortical thinning and higher CSF volumes (Dorner et al., 2018; Fletcher et al., 1992, 1996b; Khan et al., 2006; McAllister et al., 1991a). Animal hydrocephalus models were recorded to have up to 50 % compression of size in the parietal and occipital lobes (McAllister et al., 1991). The parietal and occipital cortex both myelinate approximately 4 to 6 months after birth (Deoni et al., 2011), thus if unmyelinated at the time of onset, for infants under that age, the parietal and occipital cortex may experience direct compression with little to no protection from the expanding ventricles (Dalen et al., 2006; Dennis et al., 1981a; DeSilva and Lesnik, 2008; Gammal et al., 1987). Furthermore, US studies following ventricular dilation have recorded greater expansion of the posterior occipital horns of the lateral ventricles than the anterior frontal horns (Brouwer et al., 2010). The parietal cortex's close proximity to the occipital horns will further increase its susceptibility to injury.

Damage of the posterior cortex during ventricle dilatation can cause pathologic changes to its neuroanatomical functional development. Since the posterior cortex has been associated with non-verbal learning (visuospatial skills and numeracy) (Andersen, 2011; Dehaene et al., 2003; Klingberg et al., 2002; Matejko and Ansari, 2019; Sahan et al., 2018), one should expect to see a decrease deficits in these cognitive domains if the posterior cortex is damaged (McAllister et al., 1991a). Visuospatial skills are defined as one's ability to identify, perceive, and integrate visual and spatial patterns in more than one dimension (De Vega et al., 1996; Klingberg et al., 2002). This includes skills such as shape recognition, abstract design or map tracing. Numeracy is a measure of one's numerical literacy or one's ability to understand numbers, their amounts and relationships (Brooks and Pui, 2010). Deficits in non-verbal learning in children with previous infantile hydrocephalus has been cited by multiple studies (Barnes et al., 2002; Brookshire et al., 1995; Buckley et al., 2012; Dalen et al., 2006; Dennis et al., 1981a; Dorner et al., 2018; Fletcher et al., 1992, 1996a; McAllister et al., 1991a; McAllister, 2012; Raybaud, 2017; Rourke et al., 1990; Rourke, 1995).

However, to our knowledge, non-verbal deficits caused by infantile hydrocephalus have not been related to changes in functional brain activity using task-based functional MRI (fMRI). Task-based fMRI can measure the activation of localized brain areas possibly affected, through the presentation of a specific task during the fMRI scan. Brain activation can be quantified by monitoring changes in blood oxygen levels in the brain, known as the blood-oxygen-level-dependent (BOLD) signal. The current case study will investigate how damage caused by ventricular dilatation in the posterior cortex may lead to changes in brain functional development and consequently non-verbal deficits. This will be achieved by localizing posterior cortex activity during an fMRI number comparison task as well through various behavioural assessments within the non-verbal cognitive domain.

1.6 Current Study

1.6.1 Hypothesis

OBJECTIVE: To study the behavioural outcomes and changes in functional neuroanatomical development in school-aged children with treated infantile hydrocephalus.

HYPOTHESIS: Reorganization of the posterior cortex in patients with treated infantile hydrocephalus is associated with non-verbal deficits in childhood.

RESEARCH AIMS:

1. Assessment of learning outcomes: To compare non-verbal learning (visuospatial and numeracy) outcomes in children who have experience hydrocephalus during infancy and healthy controls.

2. Parietal cortex activation: To investigate parietal cortex activation through a number comparison task in fMRI.

1.7 Study Objective

The objective of this study is to investigate the long-term neurodevelopmental outcomes of shunted patients with treated infantile hydrocephalus. We will examine the behavioural outcomes of these patients and determine whether they will have disability discrepancies in non-verbal and verbal learning. Furthermore, we will compare their blood-oxygen-level-dependent (BOLD) signal intensity in the parietal cortex during an fMRI task to healthy control children. The following study will be presented through a series of cases of individual patients with previous infantile hydrocephalus as a case study. Our current patient sample size (n=3) is primarily due to difficulties in recruiting stable hydrocephalus patients who fit the exclusion criteria of the study which included: not having a programmable (magnetic) shunt and their ability to complete all of the behavioural assessment as well as the fMRI task. Patient recruitment in longitudinal clinical studies can be especially challenging task once patients have been discharged from hospital, this is particularly true for pediatric patient populations (Boklan, 2006; Comerford et al., 2017; Denhoff et al., 2015; Ferrari et al., 2008; Glickman et al., 2008; Kadam et al., 2016; Michelson et al., 2018). Our current case study will consider the clinical history of individual patients with treated infantile hydrocephalus alongside their behavioural profiles and posterior brain activity during an fMRI number comparison task.

1.7.1 fMRI Case Study

Throughout the course of medical research history, neurological case studies have consistently shown promise in helping researchers and physicians to gain a better understanding of structure and function relationships in the brain (Danckert and Mirsattarri, 2012). Early cognitive neuroscience research in areas such as language, memory, motor and visual skills depended greatly in clinical observations of individual patients (Danckert and Mirsattarri, 2012). Such findings have laid the foundation for identifying numerous brain areas, while also mapping out future research in the field of functional neuroanatomy. The advent of neuroimaging techniques such as CT and structural MRI has allowed for scientists to link cognitive deficits with brain injuries. The introduction of fMRI provided real-time clues as to the underlining neurological mechanisms and brain activity taking place when presented with a behavioural task (Danckert and Mirsattarri, 2012), thereby making, fMRI a powerful tool for neurological case studies.

Due to issues such as image acquisition, signal to noise ratio, and large amounts of inter-subject variability, fMRI studies face major concerns in replicability, statistical power, validity and reliability (Arbabshirani et al., 2017; Dubois and Adolphs, 2016). As a result, fMRI data requires complex statistical analyses with large sample sizes in order to draw definitive conclusions (Turner et al., 2018; Woo et al., 2014a) thus, making sample size a crucial caveat in fMRI research. However, despite these restrictions, the use of fMRI in clinical case studies still shows promise when considering its potential in providing insights into neuronal mechanisms changes, cognitive deficits and treatment for the long-term care of patients with certain conditions. In recent years there has been a significant increase in publications targeting fMRI as a case study method to better understand patient populations (Arbabshirani et al., 2017; Basagni et al., 2019; de Bertoldi et al., 2015; Edes et al., 2017; Iyengar, 2016; Korsnes et al., 2009; Nemmi et al., 2015; Pizoli et al., 2011; Radman et al., 2016; Roland et al., 2017).

Researchers undertaking fMRI case studies must take into consideration various factors when designing their hypothesis, objectives, experiments, data analysis, presentation, as well as the challenges involving study power. For instance, studies should have a specific research question in regarding brain areas of interest, in order to use fMRI tasks targeting their related functions (Danckert and Mirsattarri, 2012). This can be accomplished by selecting tasks, that are well documented in the literature, with a robust BOLD signal response in specified brain areas for healthy control participants (Danckert and Mirsattarri, 2012). Tasks involving bilateral (right and left – on both hemispheres of the brain) activation should also be considered to further improve signal to noise ratio. Researchers should select simple tasks so that patients can perform them either at the same level or slightly below healthy controls. In order to measure the extent in which certain networks are activated in patients or whether alternative neuronal networks are being utilized during the given tasks. Adolph and colleagues recommend quantifying the BOLD signal response by using derived regions-of-interests (ROI) from the analyzed fMRI data of individual participants in order to compare activation pattern and trends between the participants (Dubois and Adolphs, 2016). An ROI is generally small area (usually defined by coordinates), and may include only a few voxels, (voxels being the three-dimensional unit of measurement for MRI images) (Smith et al., 2009). BOLD signal of a given ROI can be quantified by calculating the percent signal change, which is the percentage how much signal intensity in a given ROI increased during the task relative to baseline (not during the task) (Mazaika). ROI analysis will

enable us to study the possible differences in BOLD response for each participant, in areas of interest and compare activation changes between the individual patients and individual controls.

Chapter 2

2 Methods

2.1 Participants

2.1.1 Socioeconomic Status

In the following sub-sections, we will provide details with regards to the participants who were recruited for the current study, including the clinical history of the individual patients along with a list of the control participants. We will also provide information about the socioeconomic status (SES) of the parents for each participant using the Hollingshead Four Factor Scale, which measures SES through variables such as parental education and occupation (Cirino et al., 2002). The SES score can range from 8 to 66, with low SES being scores between 8 to 20 and average SES being scores between 21 to 66. Parental education was also measured using a score system of 1 to 7, described in Table 1 (Cirino et al., 2002; Yale Journal of Sociology | Sociology). Parental SES is an established variable that is often measured when studying the neurodevelopment, particularly the cognitive outcomes in pediatric patients. SES includes, but is not limited to, maternal education, single parent families, occupation, familial support, and social environment (Benavente-Fernández et al., 2019; Brookshire et al., 1995; Chin-Lun Hung et al., 2015; Lodha et al., 2018; Ritzema et al., 2018). Low SES, as well as low maternal education, and single parent families, have all been associated to adverse neurodevelopmental outcomes and cognitive impairments for preterm as well as full-term infants (Benavente-Fernández et al., 2019; Lodha et al., 2018; Ritzema et al., 2018).

Level of School Completed	Score
Less than the seventh grade	1
Junior high school (9^{th} grade)	2
Partial high school (10^{th} or 11^{th} grade)	3
High school graduate	4
Partial college (at least one year) or specialized training	5
Standard college or university graduation	6
Graduate professional training (graduate degree)	7

Table 1: The parental educational score of the Hollingshead system for SES. Ranging 1 to 7, with 1 equal to a seventh-grade education level, and 7 for graduate level degree or above.

2.1.2 Hydrocephalus Patients

The following descriptions contain the individual patient history of each of the hydrocephalus patients who were recruited in our study. A list of individual patients is described in Table 2.

Participant	Sex	Age	Maternal Education	Paternal Education	Single vs Two Parent Family	SES score
1A	M	5 years 6 months	5	6	Two	25
2A	M	9 years 11 months	6	6	Two	48
3A	M	5 years 4 months	5	3	Single	29.5
4A	M	6 years 3 months	5	6	Two	36.5
5A	M	8 years 11 months	4	3	Single	29

Table 2: The list of participant ID, sex, age at time of participation, parental education, single vs two parent family, and SES score of patients who were diagnosed and treated for hydrocephalus during infancy. All of the patients were male, their age was measured at time of participation. Patients 1A and 3A were excluded from further analysis as they were unable to complete the experimental protocol of the study.

Patient 1A was born premature with a gestational age of 25 weeks and had an extremely low birth weight of 800 grams. Patient 1A was diagnosed with bilateral IVH associated with prematurity at the time of birth. Patient 1A was serially tapped at the neonatal intensive care unit (NICU) for two months. At three months patient 1A's IVH had progressed to global ventricular dilatation and hydrocephalus they were subsequently treated with a right VP shunt. Patient 1A was aged 5.50 years (5 years 6 months) when they were recruited and had no revisions of the shunt since its initial insertion. Patient 1A was unable to complete the experimental protocol due to fear of the MRI scanner they were removed from further analysis.

Patient 2A was born to full term and at 1 month of age they developed a blood clot or thrombosis in their right transverse sinus (one of the many draining veins of the brain). The thrombosis led intracerebral bleeding and development of IVH. Patient 2A received four ventricle taps was closely monitored for any signs of progressive ventricular dilatation and hydrocephalus. At age 4 months they were diagnosed with developing hydrocephalus with the following symptoms: irritability, bulging skull sutures in the fontanelle, and increased head circumference. They were subsequently treated with a right parietal VP shunt. Patient 2A had no shunt revisions. Patient 2A was 9.92 years old (9 years 11 months) at the time of participation. The structural (preoperative and postoperative) MRI images of patient 2A are shown in Figure 6.

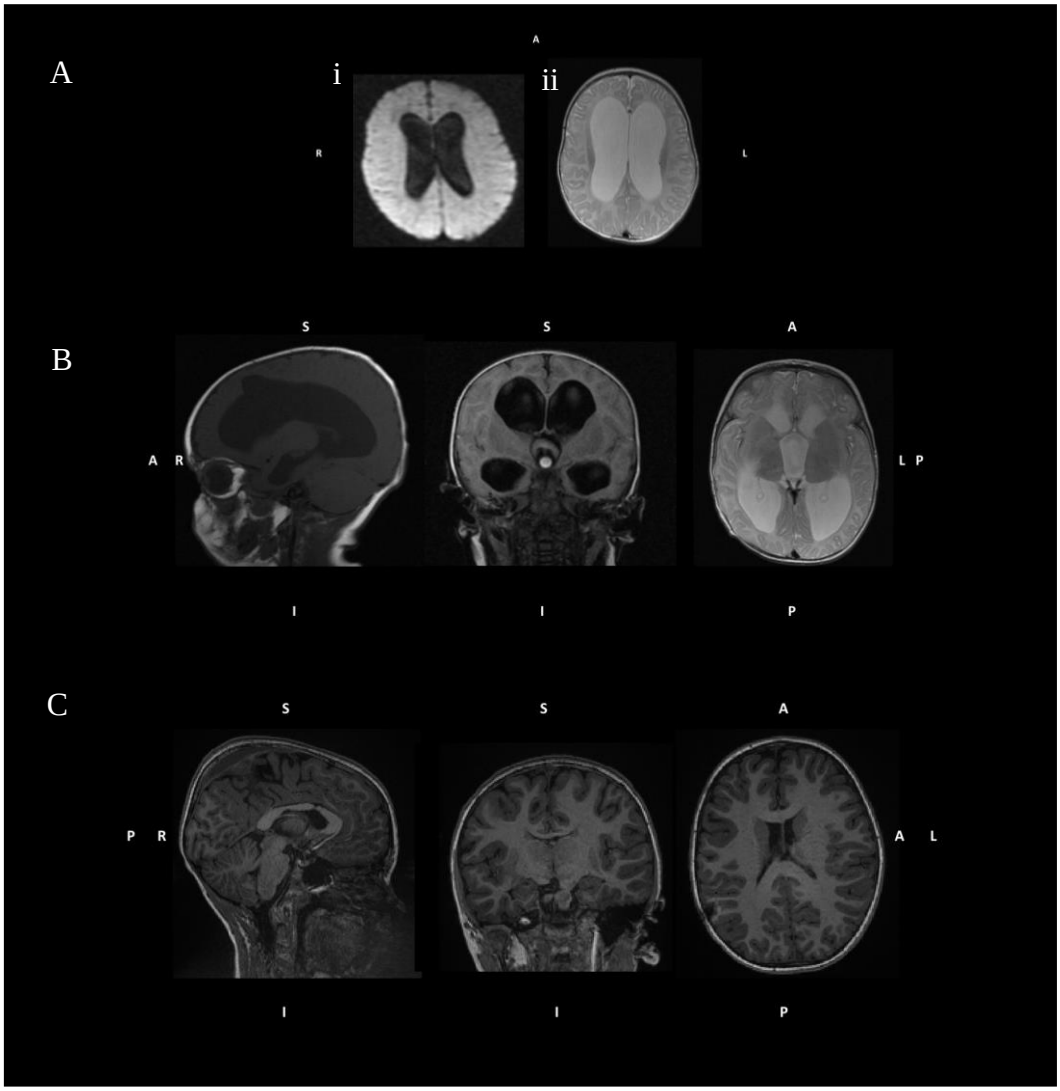

Figure 6: The structural MRI images of patient 2A, just before their VP shunt insertion (A, B) and years after surgery (C). Figure 6A shows the progression of patient 2A from moderate to severe ventricular dilatation. The T1 weighted image on the left (i) shows patients 2A at 2 months with moderate ventricular dilatation. As their condition progressed, patient 2A developed severe ventricular dilatation at 4 months, shown in the T2 weighted image on the right (ii). Patient 2A's MRI structural images, just prior to their VP shunt insertion (B), years after surgery (C) at 9 years of age. At the time of participation, patient 2A ventricles had substantially reduced in size, through continual CSF drainage provided by the VP shunt. The directions of the MRI images are indicated as superior (S), anterior (A), posterior (P), right (R), left (L), inferior (I), and posterior (P).

Patient 3A was born premature at age 27 weeks' gestation, with a very low birth weight of 1080 g and was diagnosed with hydrocephalus secondary to severe IVH (grade III) due to prematurity. Patient 3A received multiple ventricular taps, followed by the insertion of a right parietal VP shunt at 5 months in age. Patient 3A was 5.33 years old (5 years 4 months) at the time of participation they were unable to complete the experimental protocol due to fear of the MRI scanner.

Patient 4A was born to full term. At 3 weeks old, patient 4A had developed symptoms of progressive hydrocephalus including increased head circumference. They were admitted to hospital and were diagnosed with hydrocephalus secondary to Dandy-Walker malformation at 3 weeks of age. The Dandy-Walker malformation is a congenital malformation that involves the agenesis (partial or complete absence) of the cerebellar vermis, the cystic dilatation of the fourth ventricle, and the enlargement of the posterior fossa. Approximately 80% of patients with Dandy-Walker malformation develop hydrocephalus, due to the atresia (narrowing) of the foramina Luschka and Magendie which drain CSF from the fourth ventricle (Armstrong et al., 2007; Pinchefsky et al., 2019; Tully and Dobyns, 2014). Patient 4A subsequently underwent two serially ventricle taps and then had a right VP shunt inserted at 1 month, a week after their initial diagnosis of hydrocephalus. They had no shunt revisions. Patient 4A was 6.25 years old (6 years 3 months) at the time of participation. The preoperative cranial US of patient 4A, as well as their structural MRI at the time of participation is shown in Figure 7.

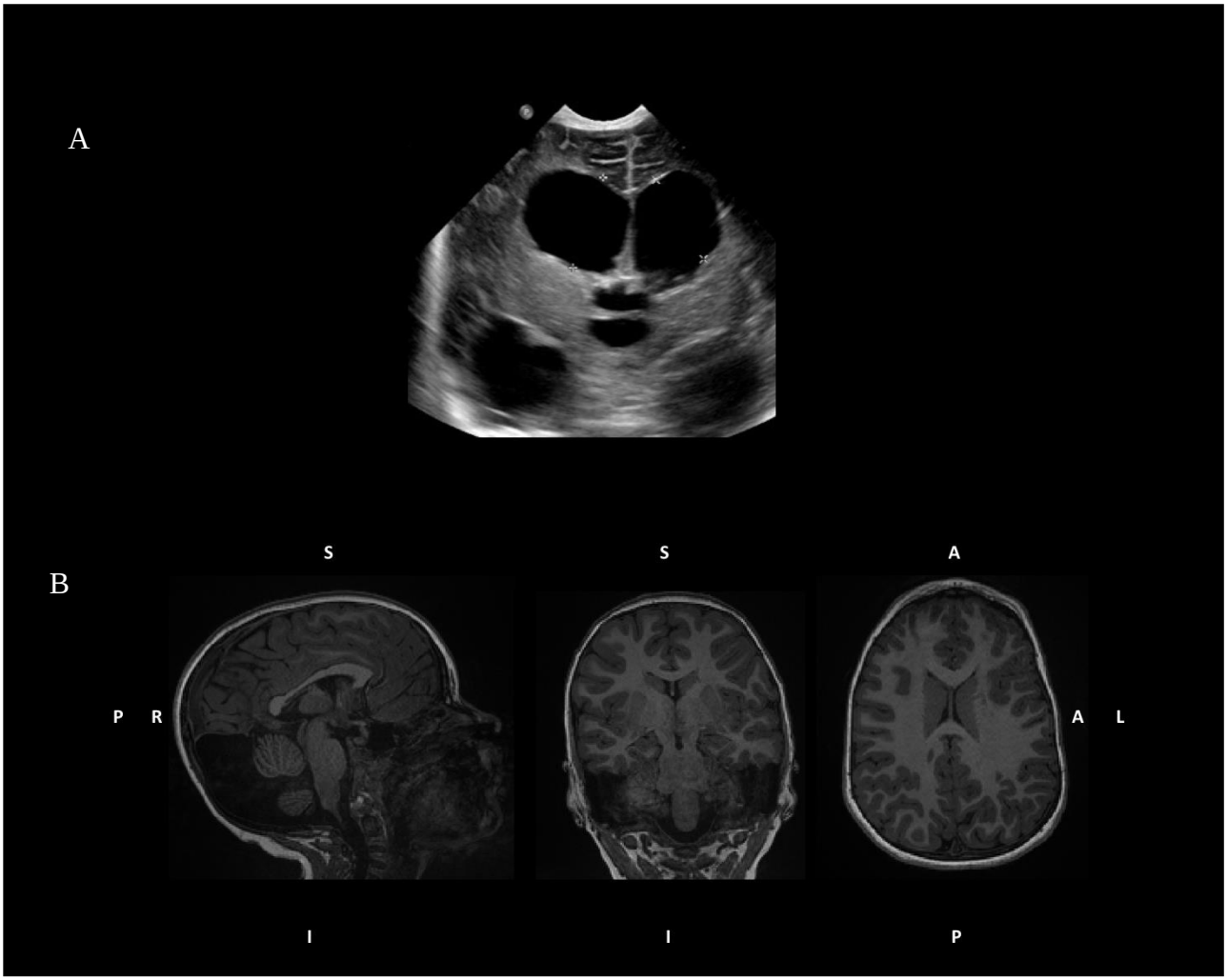

Figure 7: The preoperative coronal head US of patient 4A at 1 month (A) showing the frontal horn of the lateral ventricles. Patient 4A had severe ventricular dilatation, however due to their immediate shunt insertion, they did not have large volumes of CSF for a long period of time. The structural MRI images of patient 4A (B) show reduction of ventricle size, years following surgery, at age 6. Note, the partial formation of patient 4A's cerebellum, as well as their enlarged posterior fossa, a consequence of Dandy Walker Malformation. The directions of the MRI images are indicated as superior (S), anterior (A), posterior (P), right (R), left (L), inferior (I), and posterior (P).

Patient 5A was born premature at 26 weeks of gestation with an extremely low birth weight of 818 grams. They were diagnosed with hydrocephalus secondary to IVH as well as meningitis at the time of birth. Meningitis is the inflammation of the membranes (meninges) that surround the brain, due to usually a bacterial infection. Prior studies, have shown meningitis to have a significant association with IVH in premature neonates (Miedzińska et al., 2012). Due to their young age at the time of diagnosis, patient 5A was not shunted directly. Instead they underwent an endoscopic assisted pellucidotomy, which similar to ETV, involves creating a small hole in the septum pellucidum, a thin membrane that separates the two lateral ventricles (Mohammad and Diaz, 2017). The endoscopic assisted pellucidotomy was used to enable diversion of flow and drainage of excess CSF (Mohammad and Diaz, 2017). Patient 5A was subsequently monitored in the NICU for 5 months. Patient 5A a right VP shunt insertion at 5 months of age. They had no shunt revisions. Patient 5A was 8.92 years old (8 years 11 months) at the time of participation. The preoperative cranial US of patient 5A, as well as their structural MRI at the time of participation is shown in Figure 8.

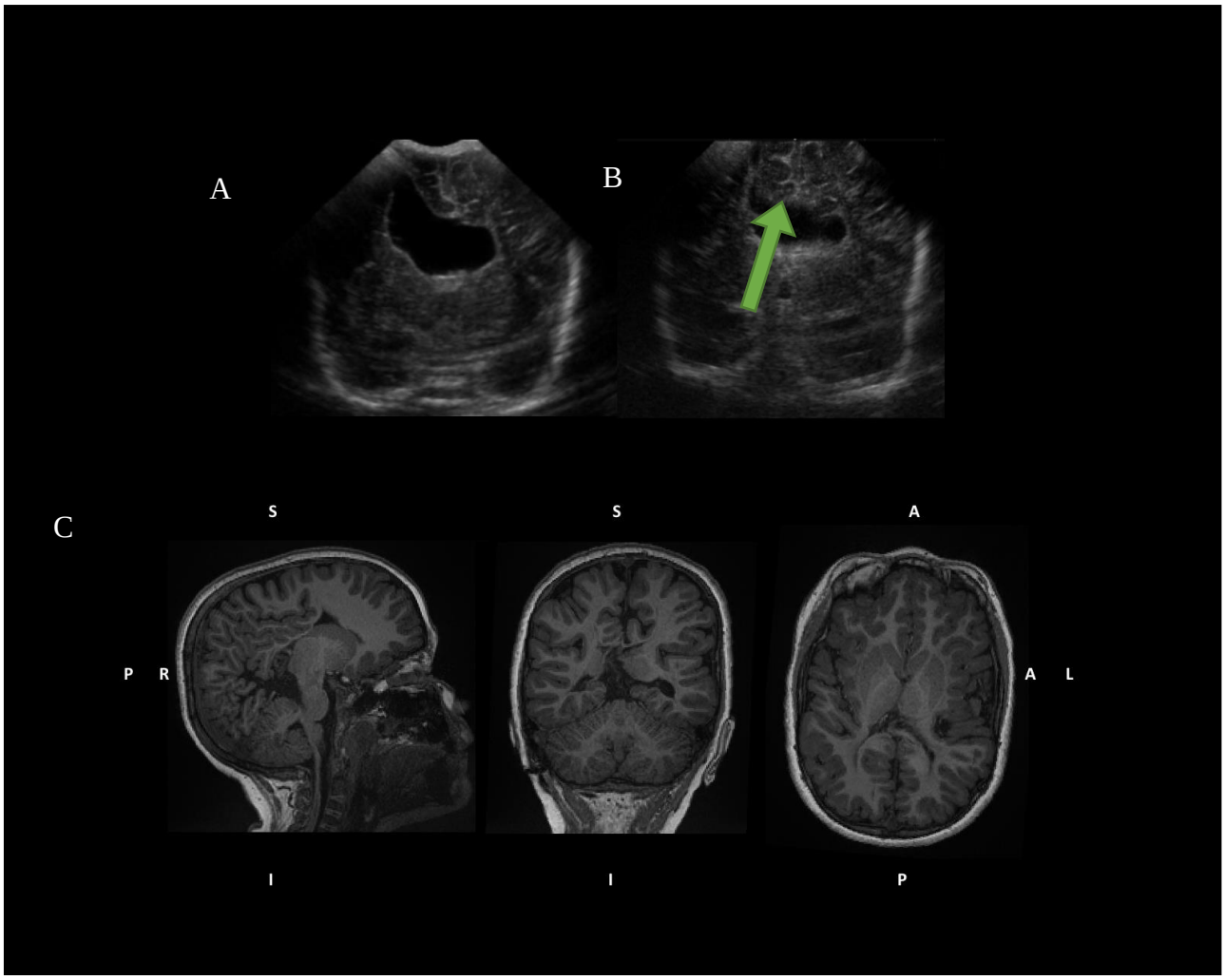

Figure 8: The preoperative sagittal head US of patient 5A at 1 month (A) showing the moderate dilatation of the frontal horns. Periventricular cysts, indicated by the green arrow, were found around the ventricles at the site of hemorrhage (B). The structural MRI images of patient 5A years following surgery, at age 8 is shown in Figure 8C. At the time of participation, patient 5A ventricles had substantially reduced in size, due to the continual CSF drainage provided by the VP shunt. The directions of the MRI images are indicated as superior (S), anterior (A), posterior (P), right (R), left (L), inferior (I), and posterior (P).

2.1.3 Control Group

Controls were recruited through the Western University's Department of Psychology Child Developmental Participant Pool. Parents of the children in the developmental pool were added during their post-natal stay in hospital after the birth of their child. They were recruited and provided with general information about the study through either email or over phone. The control group consisted of healthy children aged 4-13 years with no prior history of neurological disease. A total of 12 control participants were recruited, their mean age was 9.318 years (9 years and 4 months) with a sex ratio of 1:1. A list of the control group is displayed in Table 3.

Participant	Sex	Age	Maternal Education	Paternal Education	Single vs Two Parent Family	SES score
1B	M	11 years 0 months	6	6	Two	45.5
2B	F	13 years 1 month	6	6	Two	45.5
3B	M	10 years 7 months	7	6	Two	49.5
4B	M	8 years 10 months	7	6	Two	49.5
5B	M	6 years 9 months	7	6	Two	49.5
6B	M	12 years 6 months	6	6	Two	50.5
7B	F	7 years 6 months	7	7	Two	66
8B	F	8 years 10 months	7	6	Two	52
9B	F	4 years 11 months	7	7	Two	66
10B	F	10 years 6 months	6	4	Single	58
11B	M	12 years 10 months	6	6	Two	60.5
12B	F	10 years 6 months	7	6	Two	57

Table 3: The control group: participant ID, sex, age at the time of participation (in years and months), parental education, single vs two parent family, and SES score of each control participant. All controls completed the behavioural assessments and MRI protocol.

2.2 Experimental Protocol

Participants underwent an initial training session, using a mock MRI scanner, in order to become comfortable with the MRI environment and practice the fMRI task before entering the scanner. The mock scanner was used to ensure that the participant would be accustomed to the MRI sounds and the closed space of the scanner. To have a better understanding of the MRI scanner and its functions, participants under the age of 7 were read an MRI storybook before going into the Mock scanner, Figure 9. Two stories, titled the *Magical Tower* and the *Hidden Lighthouse* both involved a giraffe character who was being scanned and addressed essential instructions of the MRI protocol such as remaining still and how to respond to the fMRI task. By presenting the information regarding the MRI protocol through storytelling made the MRI mock scan session accessible and enjoyable for young children.

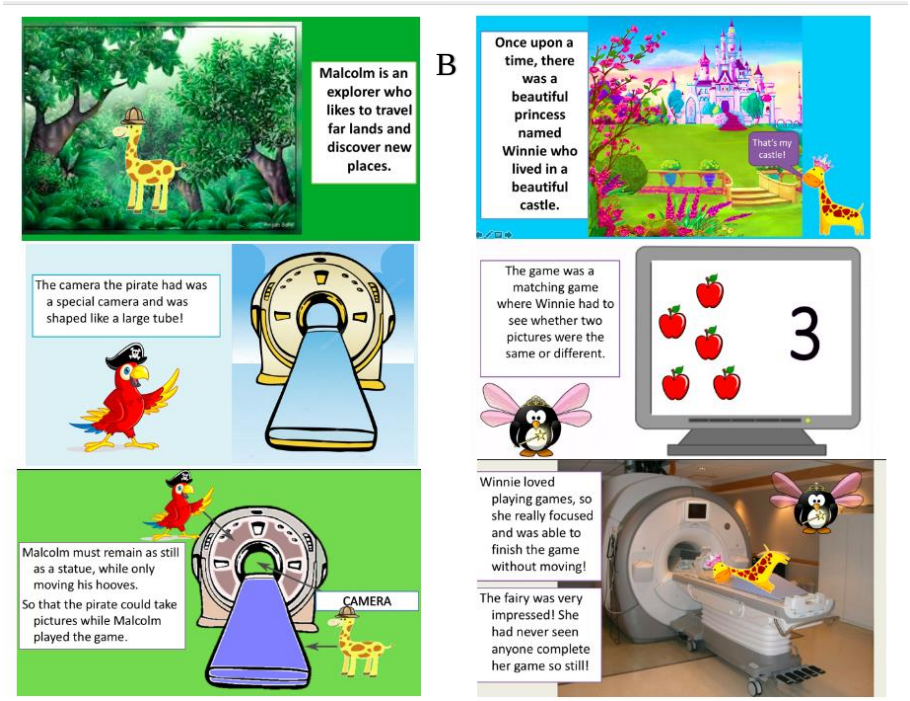

Figure 9: MRI storybook, for young children. The *Hidden Lighthouse* (A) and the *Magical Tower* (B) were created for younger participants during MRI mock scan.

After the mock scan session, which usually lasted about an hour, participants would proceed to the behavioural assessments. All of the scores of behavioural assessments were standardized to allow for across aged comparisons. All participants were assessed in the following order, subtests of the individual assessments were also listed in the order in which they were administered in. The duration of the tasks is also listed:

1) Beery Visual Motor Integration (Beery VMI)
    i. Beery VMI – 10 minutes
    ii. Visual Perception (VP) – 3 minutes
    iii. Motor Coordination (MC) – 5 minutes
2) Number Sense Screener (NSS) – 20 minutes
    - NSS was only administered to children under 7 years.
    i. Counting Skills
    ii. Number Recognition
    iii. Nonverbal Calculation
    iv. Story Problems
    v. Number Combination
3) Wechsler Preschool and Primary Scale of Intelligence (WPPSI) or Wechsler Intelligence Scale for Children (WISC) – 30 minutes
    - WPPSI was administered to children under the age of 7, and WISC was administered to children aged 7 and above.
    i. Block Design
    ii. Information
    iii. Vocabulary
    iv. Arithmetic (WISC only)
    v. Object Assembly (WPPSI only)

Once the behavioural assessments were completed, participants went into the MRI in order to acquire images of their brain and complete the fMRI number comparison task. Details

surrounding the individual behavioural tests and MRI protocol parameters will be discussed in subsequent sections.

2.3 Behavioural Assessments

In order to have an understanding of the neurodevelopmental outcomes in children with previous infantile hydrocephalus, we conducted an assortment of behavioural tests which assessed for multiple non-verbal cognitive domains such as motor, numeracy, and visual perception skills, as well as verbal learning. All behavioural test had standard scores for across age comparison. To measure the performance of the hydrocephalus patients, they will be compared to the control group and the mean standard for the normed scores. The following assessments were included in the current case study: Beery VMI, WPPSI, WISC, NSS.

2.3.1 Beery Visual Motor Integration

The Beery-Buktenica Developmental Test of Visual Motor Integration (Beery VMI) is a behavioural assessment which measures how visual processing coordinates with fine motor movements, in a process known as visual-motor integration (Beery et al., 2010; Bolk et al., 2018). Beery VMI can be used for children ages 2 and above and consists of three subtests: visual motor integration (VMI), visual perception and motor coordination (Beery et al., 2010). In the VMI subtest, participants were asked to copy a series of 30 images from a simple line to complex geometric shapes (Beery et al., 2010). A short form of the VMI subtest with 21 images was administered to participants under 7 years of age (Beery et al., 2010). In the visual perception subtest, participants were again given a sequence of shapes with increasing complexity. They were asked to match each shape's identical match from a group of three similar shapes. This subtest contained 30 items and was under timed conditions participants were given 3 minutes to complete the task. The visual perception subtest was designed to assess how well the visual system is perceiving or understand the visual information it receives (Beery et al., 2010). Lastly, the motor coordination subtest was to measure the participants' fine motor skills. Participants were asked to trace specific shapes while remaining within the given border. The motor coordination was timed participants were given 5 minutes to complete the task containing 30 items (Beery et al., 2010). All raw scores were converted to standard scores, using age-norms

of matched year and month. Standard scores, summarized in Table 4, were used to measure performance.

Standard Scores	Performance	% of Age Group
>129	Very High	2
120-129	High	7
110-119	Above Average	16
90-109	Average	50
80-89	Below Average	16
70-79	Low	7
<70	Very Low	2

Table 4: Standard scores of VMI, visual perception and motor coordination. The mean standard score was 100 with a standard deviation of 15. Relative performance (high, average, low) was assessed by the converted standard scores. The "% of age group" is the percentage of individuals who achieved a particular standard score range (Beery et al., 2010).

2.3.2 Wechsler Preschool and Primary Scale of Intelligence and Wechsler Intelligence Scale for Children

Depending on the participant's age at the time of testing they were either administered the Wechsler Preschool and Primary Scale of Intelligence (WPPSI) or Wechsler Intelligence Scale for Children (WISC). Participants under the age of 7 were administered WPPSI, and participants aged 7 or older were administered WISC (Syeda and Climie, 2014; WISC-V; WPPSI-IV). Both batteries are designed to determine a child' s general intelligence and whether developmental deficits may be present. The WPPSI and WISC contain multiple subtests that address different cognitive domains such as verbal fluency or non-verbal ability, that can provide researchers with an assessment of an individual's full scale IQ (Syeda and Climie, 2014). In the current study we will utilize selective subtests that assess non-verbal and verbal skills, in order to direct testing measures that fit the hypothesis in question, as well as to reduce testing time, since full cognitive batteries often take hours to administer and coupled with the fMRI training and testing, it would be impossible for participants to complete testing in one session. Thus, to shorten administration

time, we selected a short list of subtest or subtests, listed in Table 5, from both WISC and WPPSI.

	Block Design	Information	Vocabulary	Arithmetic	Object Assembly
WISC	✓	✓	✓	✓	
WPPSI	✓	✓	✓		✓

Table 5: Administered subtests of the WISC and WPPSI. Note the check marks indicate which subtest was a part of the respective battery.

During the block design subtest, participants were asked to reproduce an image using plastic coloured blocks. The block design subtest measures nonverbal concept formation such as abstract design, visuospatial processing, and motor coordination (Syeda and Climie, 2014; WISC-V; WPPSI-IV). For the information subtest, participants were asked a series of general knowledge questions in subjects such as science, history and geography (WISC-V; WPPSI-IV), in order to examine long-term memory and acquired knowledge. The vocabulary subtest participants were asked to define terms to measure their verbal fluency, word knowledge, word usage, and concept formation. The object assembly subtest, available only in WPPSI, was used to measure abstract design, spatial processing, and visual perception (WPPSI-IV). Here, participants were given puzzle pieces of various items and were asked to construct them. Lastly, the arithmetic subtest, administered through the WISC, measured mathematical ability through mental math problems (WISC-V). All raw scores of the WPPSI and WISC, were converted to scaled scores (Table 6), using age-norms of matched year and month.

Scaled Score	Number of SDs from the Mean	Percentile Rank Equivalent
19	+3	99.9
18	$+2\frac{2}{3}$	99.6
17	$+2\frac{1}{3}$	99
16	+2	98
15	$+1\frac{2}{3}$	95
14	$+1\frac{1}{3}$	91
13	+1	84
12	$+\frac{2}{3}$	75
11	$+\frac{1}{3}$	63
10	0 (Mean)	50
9	$-\frac{1}{3}$	37
8	$-\frac{2}{3}$	25
7	-1	16
6	$-1\frac{1}{3}$	9
5	$-1\frac{2}{3}$	5
4	-2	2
3	$-2\frac{1}{3}$	1
2	$-2\frac{2}{3}$	0.4
1	-3	0.1

Table 6: Scaled scores of WPPSI and WISC subtests. The mean standard score was 10 with a standard deviation of 3. The number of standard deviations (SD) from the mean scaled score as well as the percentile rank equivalent are also listed (WISC-V; WPPSI-IV).

2.3.3 Number Sense Screener

The Number Sense Screener (NSS) was used to evaluate numerical ability in younger participants under the age of 7 who were not administered the arithmetic subtest of the WISC (Brookes Publishing: Number Sense Screener™ (NSS™) Set, K–1, Research Edition). NSS can be divided into the following categories: numbers, relations, and operations. Each category contained a number of subtests that participants were asked to complete, listed below:

- Numbers
  - Counting
  - Number recognition
- Relations
  - Number comparisons
- Operations
  - Nonverbal calculations
  - Story problems
  - Number combinations

The counting subtests involved participants counting black stars. For the number recognition task, participants were asked to identify symbolic numbers such as the 37. During the nonverbal calculations, non-symbolic number representations in the form of black tokens, were provided. Here participants were asked to either subtract or add black tokens being removed or inserted into a box. The participant would answer by selecting one of four images of the black tokens. In the story problem subtest, participants were asked to answer word problems such as "Jill has two pennies. Jim gives her 1 more penny. How many pennies does Jill have now?" (Brookes Publishing: Number Sense Screener™ (NSS™) Set, K–1, Research Edition). The story problems involved both addition and subtraction. Lastly, in the number combination subtest, participants were asked addition and subtraction questions such as "How much is 7 take away 3?" (Brookes Publishing: Number Sense Screener™ (NSS™) Set, K–1, Research Edition). Participants were provided with aids (pencil and paper, number list – series of 10 black dots) to assess them in answering questions during the story problem and number combination subtests. Raw scores were converted to standard scores using the respective grade of the participant (junior kindergarten, senior kindergarten or grade 1).

2.4 Neuroimaging

2.4.1 Functional Magnetic Resonance Imaging

As mentioned in chapter 1, fMRI, can be used to measure brain activity through changes in blood oxygen levels in the brain, by acquiring the respective BOLD signal (Ulmer, 2013). The association of BOLD signal with brain activation is drawn on the assumption that activation of neurons in the brain is associated with changes in blood flow, in a hemodynamic response, as seen in Figure 10 (Magnetism; Ulmer, 2013). When studying brain activation using fMRI one can consider either use resting state or tasked based fMRI (Zhang et al., 2016). In a resting state fMRI, measurements of brain activation are taken at "rest" where there is no task given to participants. Here, researchers wish to assess global connectivity of resting state networks or distal brain areas (Lv et al., 2018; Pizoli et al., 2011; Roland et al., 2017; Smyser et al., 2013; Thompson, 2018). For task fMRI, participants are given a specific task to do during the actual scan, in order to study specific brain regions associated with that task. For example an fMRI motor task could be designed to measure activation and localize the motor cortex (Zhang et al., 2016).

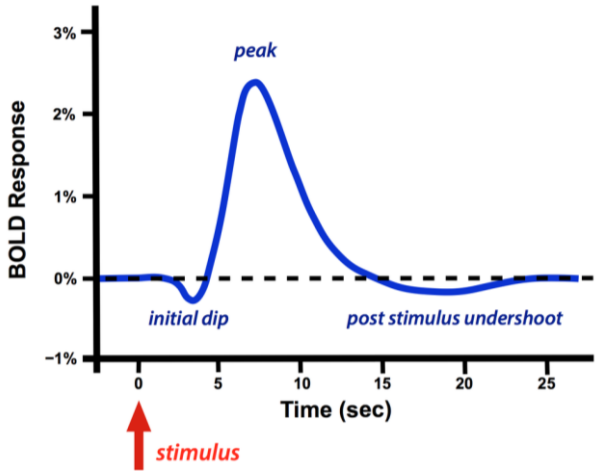

Figure 10: Blood-oxygen-level dependent (BOLD) signal used to measure brain activation in fMRI (Ekstrom, 2010; Magnetism; Ulmer, 2013). This graph illustrates the changes in blood oxygenated levels due to neuronal activation which can be correlated to signal on the recorded fMRI image. The initial dip is due to an initial increase in deoxygenated blood, which is followed by positive response due to an increase in oxygenated blood, leading to a peak in signal. The under-shoot is caused by a decrease in blood volume.

2.4.2 MRI parameters

Functional and anatomical brain images were acquired using a Siemens MAGNETOM Prisma whole-body 3 Tesla MRI scanner with a 32-channel head coil at the Robarts Research Institute's Centre of Functional and Metabolic Mapping (CFMM). High resolution anatomical T1 contrast images were measured through magnetization prepared rapid gradient echo (MP-RAGE) pulse sequence, with the following parameters: repetition time (TR) = 2300.0 ms, echo time (TE) = 2.93 ms, flip angle = 9 °, field of view (FOV) = 256 mm, sagittal interleaved slices with a voxel thickness of 1.0 mm × 1.0 mm × 1.0 mm. Functional images were acquired through an echo planar (ep) image pulse sequence with the following parameters: TR = 1000.0 ms, TE = 30.00 ms, flip angle = 40 °, FOV = 208 mm, SNR 1.00, sagittal interleaved slices with a voxel thickness of 2.50 mm x 2.50 mm x 2.50 mm. Please refer to Appendix A for more information about the MRI protocol (Appendix A – MRI CFMM Protocol).

2.4.3 Task Paradigm

The fMRI task used was adopted from a 2012 study conducted by Jessica Cantlon and colleagues at Rochester University (Emerson and Cantlon, 2012). Cantlon et al., hypothesized that functional connectivity between brain regions recruited during numerical matching and is a predictor of mathematical performance. We modified the task to make it more accessible for young children. During the fMRI comparison task, participants were presented different items (numbers, faces, or shapes) and were asked to identify whether they were the same or different. The two images were presented left and right of the monitor and had a central cross between them. Participants were given two buttons while in the scanner and were instructed to press either right button for same items or left button for different items. E-Prime 2.0 Standard was used to create the task (E-Prime 2.0).

The task was created in order to localize number-related BOLD signal response in brain areas associated with non-verbal learning specifically numeracy. Number items were presented using both non-symbolic representation (dots, items, etc. – using amounts to represent numbers) and symbolic representation (Arabic numeral – using symbols to represent numbers such as 2, 7, etc.) (Mussolin et al., 2010). During the number condition, participants were asked to determine whether symbolic numbers was equal to the non-symbolic representation, shown in Figure 11A.

For the face condition, participants were presented with grey-scale pictures of various smiling children wearing caps (Dalrymple, K.A., et al.). The faces were presented with front and side view. All face pictures were provided by Dartmouth Database of Children's Faces (Dalrymple, K.A., et al.). Pairs of black shapes that were either identical or different was also presented. The number and shape stimuli were used to localize non-verbal related activation in posterior brain regions, particularly the parietal cortex. The faces stimuli were used as a control. Participants were given either 3 or 6 seconds to respond to each pair. With 25 seconds of rest in between each block of 7 pairs, in which they were presented with a cross. The task ran for approximately 10 minutes. The individual stimuli used is summarize in Figure 11.

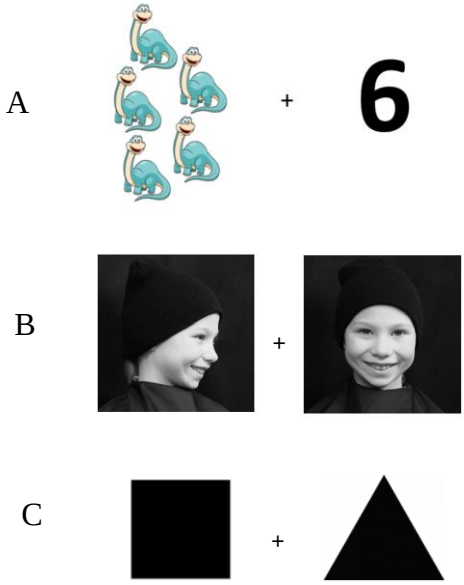

Figure 11: Example the stimuli given during the fMRI comparison task numbers (A), faces (B), and shapes (C). Images of the child faces were provided by Dartmouth Database of Children's Faces (Dalrymple, K.A., et al.).

2.5 Data Analysis of fMRI data

2.5.1 Preprocessing

The fMRI data was analyzed using FMRIB Software Library (FSL) (Smith et al., 2001). Data files collected from the scanner were initially sorted and converted from their initial Digital Imaging and Communications in Medicine (DICOM) format into Neuroimaging Informatics Technology Initiative (NIfTI) using the Brain Imaging Data Structure's (BIDS) dcm2bids application (Gorgolewski et al., 2016). Timing files relating to stimuli presentation were created depending on number of volumes acquired. All of the structural and functional images underwent standard computational preprocessing steps to reduce variability in the data not related to the experimental design or research question, and also increase the signal-to-noise (SNR) ratio (Huettel et al., 2014). Preprocessed data underwent the following steps: skull stripping of structural data files through FSL's Brain Extraction Tool (BET) (Smith, 2002; Smith et al., 2001). Thereafter the 3D functional images were concatenated to 4D using fslmerge. Through FMRIB's Easy Analysis Tool (FEAT) (Smith et al., 2001; Woolrich et al., 2001, 2004), data files completed the remaining preprocessing steps by undergoing high pass filtering of 100 Hz (an interval of 0.01 seconds), rigid-body motion correction, slice time correction, spatial smoothing using 5 mm – full-width at half maximum (FWHM) Gaussian kernel, and prewhitening. Prewhitening is used to remove task-unrelated noise. The fMRI data was then overlaid with or coregistered to high-resolution anatomical images, using boundary-based registration (BBR) (Greve and Fischl, 2009), using linear transformations with 6 degrees of freedom (DOF). Images were then normalized into standard MNI (Montreal Neurological Institute) space using the NIHPD Objective 1 atlases pediatric brain atlas (Evans, 2006; Fonov et al., 2011). In order to reduce normalization errors from using adult template from morphological changes due to age and development, as the cerebral cortex matures in childhood (Fonov et al., 2011). Due to small sample size, we used a single age range template for normalization and selected the 4.5 – 18. 5 years symmetrical atlas for all analyzed participants. We used non-linear transformation with 12 DOF. The pediatric atlas was created by a database of 324 children who had enrolled in the MRI Study of Normal Brain Development (NIHPD) funded by the National Institute of Health (NIH) in the United States in partnership with MNI (Evans, 2006; Fonov et al., 2011).

2.5.2 First Level Analysis

The general linear model (GLM) was used to analyze the functional data collected during the number comparison task. FEAT's first level analysis tool was used to conduct the first level analysis (Woolrich et al., 2001) of the functional data. The experimental stimuli or explanatory variables (EVs), which included: numbers, faces and shapes were used to set up the GLM. Contrasts of each of the stimuli were set up in order to determine brain activity during the specific stimuli when then other stimuli were not present. In order to study which brain areas were activated during each of the different stimuli. The number contrast was created by contrasting the number stimuli with the faces and shapes, in which numbers was greater than all of other stimuli (numbers > faces & shapes). Two other contrasts were also created: the shape contrast (shapes > numbers & faces) and the face contrast (faces > numbers & shapes). The setup of the each of the contrasts is shown in Table 7.

Contrast			Stimuli		
			EV1 numbers	EV2 faces	EV3 shapes
COPE 1	Numbers > Shapes & Faces	number contrast	2.0	-1.0	-1.0
COPE 2	Faces > Numbers & Shapes	face contrast	-1.0	2.0	-1.0
COPE 3	Shapes > Numbers & Faces	shape contrast	-1.0	-1.0	2.0

Table 7: List of the contrasts or the linear combination of parameter estimates (COPE) of the GLM. The two-hypothesis contrast were designed to localize posterior activation: number contrast (numbers > faces & shapes), and shape contrast (shapes > numbers & faces). The face contrast (faces > numbers & shapes) was used as a control contrast.

Cluster-based thresholding was used to determine activated brain areas during the individual contrast, with a z statistic threshold of 3.1 and p value of 0.001 FWE (family wise error rate) corrected for multiple comparisons based on the recommendations of Woo and colleagues (Woo et al., 2014b) for smaller sample sizes. In order to reduce the likelihood of obtaining false activated clusters (type I errors) (Huettel et al., 2014; Woo et al., 2014a).

2.5.3 Second and Group Level Analysis

Group level analysis was conducted for the control group to determine mean activation for the each of the given contrasts. Single subject second level analysis was conducted for the patients, in order to normalize the activated clusters to MNI space. Fixed effects model was used, as the sample size is too small to make inferences about the greater population using a mixed effects analysis (Worsley et al., 2002). The cluster-base z statistic threshold was set to 3.1 with a p = 0.001 (FWE corrected). Significant clusters were mapped onto the brain templates for the control group and individual patients. Both the group and second level analyses were conducted using FEAT's Higher-level analysis tool (Woolrich et al., 2004).

2.5.4 Region of Interest Analysis

Through the functional MRI analysis, we were able to localize brain activity, as BOLD signal intensity, in the parietal cortex during the number contrast. Significant clusters for each of the contrast were found using FSLeyes' FEAT mode (McCarthy, 2019). In order to quantify BOLD signal response a region of interest (ROI) analysis was conducted. The primary goal of the ROI analysis is to compare activation trends, in percent signal change, in small areas of interest (ROI) between each participant, during the three different contrasts (number, face, and shape contrasts) of the study. For the ROI analysis, we were interested in small areas of interest, using specific MNI coordinates where the significant clusters experienced peak activation for the control group. Since we had already normalized all of the functional data into MNI space, during the preprocessing steps, we were able to extract ROIs through their MNI coordinates [X Y Z]. The MNI coordinates were identified by classifying their Brodmann's area using the MNI to Talairach online tool and Brodmann's Interactive Atlas (Brodmann's Interactive Atlas; The MNI <-> Talairach Tool; Lacadie et al., 2008). The number contrast (numbers > shapes & faces) had derived ROIs in the left intraparietal sulcus (IPS) [-32 -68 43], right IPS [32 -68 42], left superior parietal lobule (SPL) [-32 -73 53] and right SPL [32 -68 37]. All of the ROIs used are listed in Table 8. For the ROI analysis, spherical masks with 5 mm radius (approximately 2 voxels) were created in order to calculate mean percent signal change in BOLD signal response during each of the contrasts for each participant. The ROI analysis was conducted by FSL's Featquery tool (Smith et al., 2001).

Regions of Interest	MNI Coordinates [X Y Z]
Left IPS	[-32 -68 43]
Right IPS	[32 -68 42]
Left SPL	[-32 -73 53]
Right SPL	[32 -68 37]

Table 8: The MNI coordinates of the derived ROI from the fMRI analysis of the number (numbers > shapes & faces) contrast.

Chapter 3

3 Results

3.1 Behavioural Results

The raw scores for all the behavioural assessments were converted to standard scores, based on the participant's age in years and months, to allow for across age comparisons, as mentioned in section 2.3. The hydrocephalus patients: 2A, 4A, and 5A individual standard scores were compared to the mean scores of the control group. The mean standard scores of the norms were also used in order to measure level of performance in the behavioural assessments, with high performance being above the mean, average being approximately equal, and low performance being less than the mean.

3.1.1 Beery VMI

The results of Beery VMI full battery can be seen in Figure 12, for the control group and the individual hydrocephalus patients. The three subtests: visual-motor integration (VMI), visual perception and motor coordination, are shown individually in each of the color bars. The mean standardized score was 100 ($\sigma = 15$) and is displayed through the black horizontal line. The control group mean displayed average performance in all of the subtests, with scores of 108.08 in VMI, 103.58 in visual perception, and 107.33 in motor coordination. Recall from Table 4, that scores between 90-109 are considered average. Patient 2A exhibited low performance in the VMI and below average performance in visual perception with a very low standard core of 56 in the motor coordination subtest. Patient 5A had low scores in all of the subtests, displaying low performance, in the VMI, to very low performance, in the visual perception and motor coordination. Interestingly, patient 4A had average standard scores in VMI, and above average performance in the visual perception and motor coordination subtests. Patient 4A had slightly higher standard scores than the control group in all of the subtests.

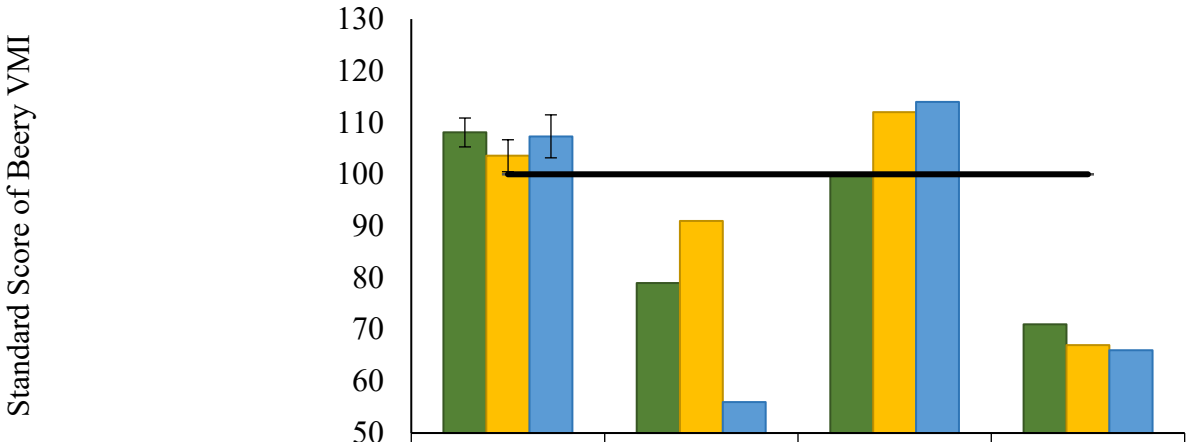

	Control Group	Patient 2A	Patient 4A	Patient 5A
Visual Motor Integration	108.0833333	79	100	71
Visual Perception	103.5833333	91	112	67
Motor Coordination	107.3333333	56	114	66
Mean Standard Score	100	100	100	100

Figure 12: The standard scores of Berry VMI assessment for hydrocephalus patients (2A, 4A, and 5A) and the control group, shown in the above bar graph. The standard scores are also listed in the table. We observed lower performance in Beery VMI for patients 2A and 5A and above average performance for patient 4A. The mean standard score (100) of the norms is represented by the black horizontal line. The standard error of the control group mean standard scores are indicated by the error bars.

3.1.2 WISC and WPPSI

Selective subtests of WISC and WPPSI (information, vocabulary, block design, arithmetic, and object assembly) were administered to participants. Raw scores were converted into scaled scores based on the participant age in years and months. Participants over the age of 7 years were administered the WISC. The results of the WISC for patients 2A and 5A as well as the control group (mean score) are shown in Figure 13. The information, and vocabulary subtests were used for verbal assessment. While the block design and arithmetic subtests were used for non-verbal cognitive assessment. The mean scaled score of 10 ($\sigma = 3$) is displayed as the black horizontal line, represents average performance, with a percentile rank of 50 (Table 6). The control group displayed average performance, with scores near the mean scaled score in the verbal subtests, and above average performance in the non-verbal subtests.

Generally, patients 2A and 5A displayed extremely low scaled scores in both of the non-verbal subtests (block design and arithmetic). Having much lower scores than the control group mean score and the mean scaled score of the norms (Figure 13). Patient 2A had a scaled score of 7 in the block design subtest (16th percentile) and a scaled score of 6 (9th percentile) in the arithmetic subtest. For the verbal subtest, patient 2A had average scores in the vocabulary subtests and below average scores in the information subtest. Patient 5A had a scaled score of 6 in the block design subtest (5th percentile) and a scaled score of 5 (9th percentile) in the arithmetic subtest. However, unlike patient 2A, patient 5A also displayed low scores in the verbal subtests as well. Though patient 5A's non-verbal test scores were still lower than their verbal test scores, aligning with our predictions.

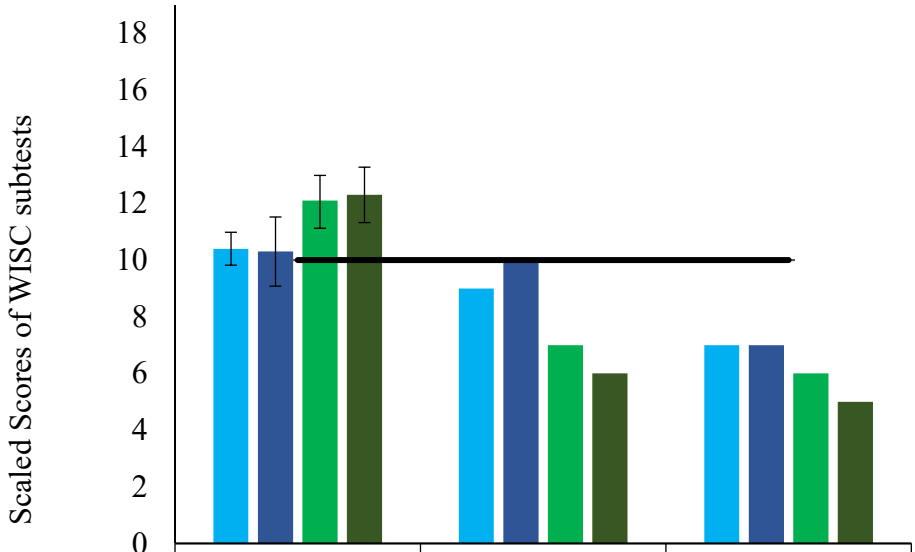

	Control Group	Patient 2A	Patient 5A
Information	10.4	9	7
Vocabulary	10.3	10	7
Block Design	12.1	7	6
Arithmetic	12.3	6	5
Mean Scaled Score	10	10	10

Figure 13: The scaled scores of selected subtests in the WISC for patients 2A, patient 5A and the control group. The mean scaled score is represented by the black horizontal line. The verbal subtests (information and vocabulary) are indicated in blue, while the non-verbal subtests (block design and arithmetic) are indicated in green. Lower scaled scores were found in the non-verbal subtests in WISC for hydrocephalus patients (2A and 5A),

and average performance for the control group. The standard error of the control group mean scaled scores are indicated by the error bars. The scaled scores of the patients (2A and 5A) and the control group are also listed in the table below the bar graph.

Participants under the age of 7 years old were administered selective subtests of the WPPSI cognitive battery. The selected subtests were information and vocabulary for verbal cognitive assessment, and block design and object assembly for non-verbal cognitive assessment. The results of the WPPSI are shown in Figure 14 for patient 4A and the control group (group mean scaled score). The mean scaled score of the norms 10 ($\sigma = 3$), is represented by the black horizontal line. The control group had high scaled scores in all of the administered subtests. Patient 4A displayed average performance in the block design and information subtests having a score of 10 in both, which is the equivalent to 50^{th} percentile (Table 6). Interestingly, patient 4A scored highly in object assembly subtest, having a scaled score of 13 (84^{th} percentile) and had a low score in the vocabulary subtest of 6 (9^{th} percentile). Which goes against predicted results, as well as trends displayed by patient 2A and 5A in the WISC. Though patient 4A displayed lower performance in all of the subtests when compared to the control group, who displayed high performance in all subtests Figure 14.

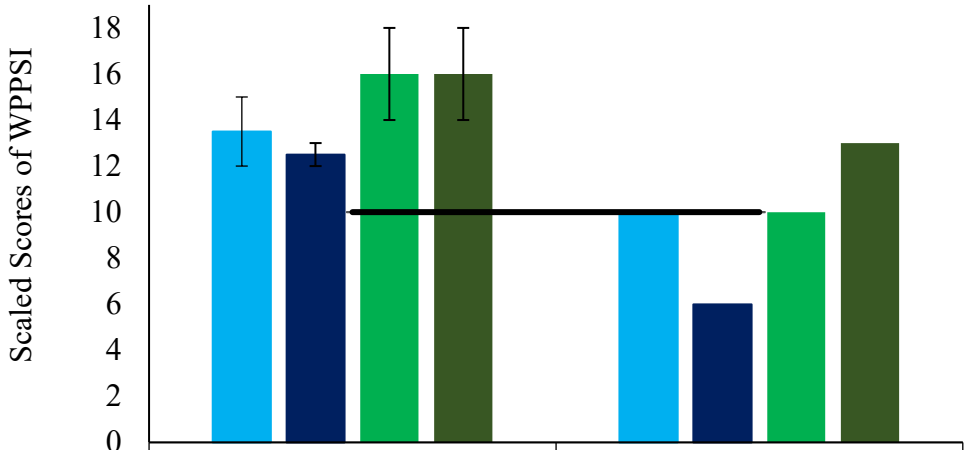

	Control Group	Patient 4A
Information	13.5	10
Vocabulary	12.5	6
Block Design	16	10
Object Assembly	16	13
Mean Scaled Score	10	10

Figure 14: The scaled scores of selected subtests in the WPPSI for patient 4A and the control group. The mean scaled score is represented by the black horizontal line. The verbal subtests (information and vocabulary) are indicated in blue, while the non-verbal subtests (block design and arithmetic) are indicated in green. Patient 4A had average scaled scores in the block design and information subtests. While having low scaled scores in the vocabulary subtest and high scores in the object assembly subtests. The standard error of the control group mean scaled scores are indicated by the error bars.

3.1.3 NSS

The NSS was administered to participants under the age of 7, to function as a mathematics assessment for participants who did not conduct the arithmetic subtests of the WISC. The results of the standard scores of younger control group and patient 4A for the NSS is displayed in Figure 15. The mean standard score is displayed by the black horizontal line (100, $\sigma = 15$). The control group ($n = 2$) had a mean standard score of 115.5 ($s = 17.678$), which translates to 77.5^{th} percentile performance, according to the norms of NSS. Patient 4A had a standard score of 110, which translates to 75^{th} percentile. The control group and patient 4A displayed similar NSS performance, this also aligns with patient 4A's performance in the Beery VMI.

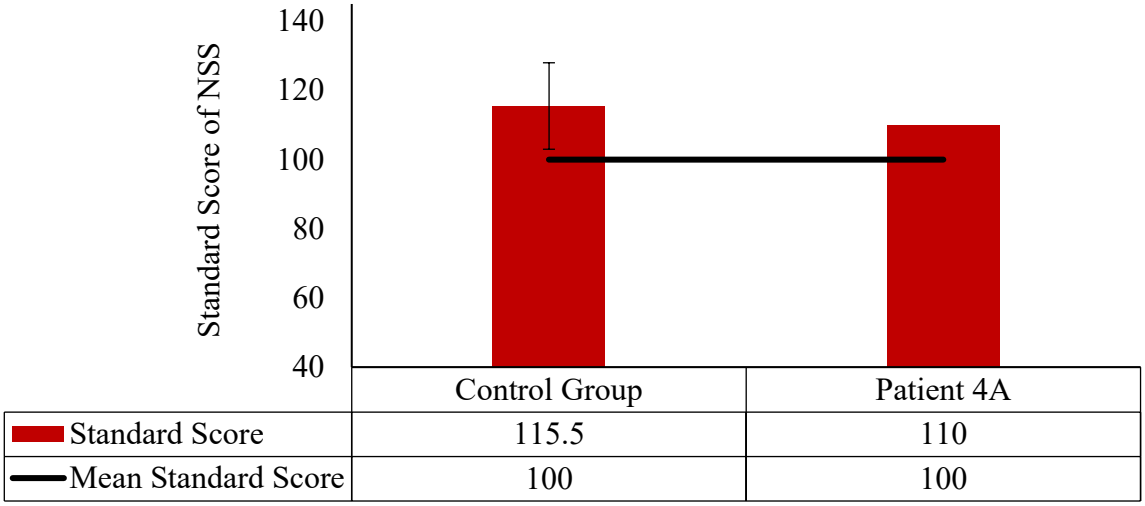

Figure 15: The standard scores of NSS for patient 4A and control group. Similar standard scores, of average performance, were displayed in both patient 4A and control group. The mean scaled score is represented by the black horizontal line. The standard error of the control group mean standard score is indicated by the error bar.

3.2 Parietal Cortex Activation

3.2.1 Number Contrast

Parietal brain activation during the number contrast (numbers > shapes & faces) is displayed in Figure 16 for the control group and each of the patients (2A, 4A and 5A). The z-masks of the significant clusters in the left intraparietal sulcus (IPS) (MNI coordinates [-32 -68 43]) for the control group and patient 2A, the right IPS (MNI coordinates [39 -82 32]) for patient 4A, and the right superior parietal lobule (SPL) (MNI coordinates [18 -73 48]) for patient 5A. Both the bilateral SPL and IPS, have been associated with numeracy in multiple fMRI studies (Ansari, 2008; Ansari et al., 2005; Arsalidou et al., 2018; Dehaene et al., 2003; Mock et al., 2018; Sahan et al., 2018). Activation signal intensity was displayed using the color bar, with lower signal (z-statistic) being red and higher signal (z-statistic) intensity being yellow.

The control group had the highest signal intensity, in the left SPL (MNI [-32 -73 53]). The SPL has been previously been associated with: non-symbolic number sets with small differences in magnitude, visual attention, number comparison tasks, and visuospatial working memory (Arsalidou et al., 2018). The hydrocephalus patients (2A, 4A, 5A) did display parietal activity, in both the IPS and SPL during the number contrast as well, though not with the same intensity or cluster size as the control group, having both weaker signal intensity and smaller clusters than the control group. This may be a consequence of statistical differences between single subject and group level analyses. To have a better understanding of patient and control parietal BOLD signal intensity differences, with quantified results an ROI analysis was conducted.

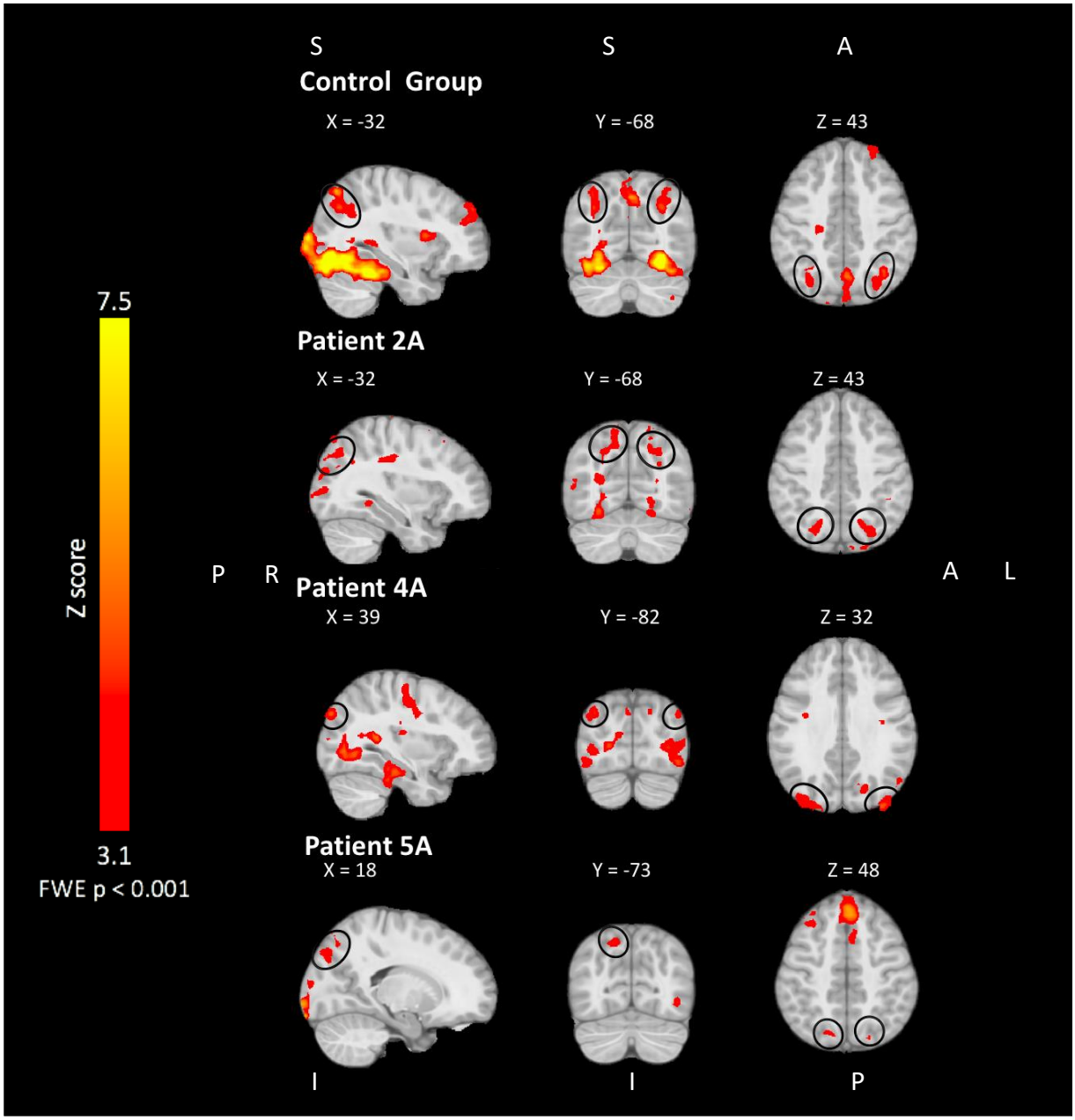

Figure 16: Parietal cortex activation during the number contrast: activated clusters in the bilateral IPS (control group, patient 2A, patient 4A) and right SPL (patient 5A) activation during the number comparison task. The above figure displays the results of a cluster-based analysis for the contrast numbers > faces & shapes (FWE corrected, p < 0.001), all of which were normalized to MNI [X Y Z]. The panel shows the activation masks are in (left to right) sagittal, coronal, axial view. The directions are indicated by superior (S), anterior (A), posterior (P), right (R), left (L), inferior (I), and posterior (P). Brain signal intensity was displayed using the color bar, with lower signal (z-statistic) being red and higher signal (z-statistic) intensity being yellow.

3.3 ROI Analysis

The results of the cluster-based analysis displayed activated brain areas for the individual patients (2A, 4A, and 5A) and the control group, at the given threshold. We localized the parietal cortex activity during the number contrast. In order to quantify the BOLD response, we will consider an ROI analysis of 4 different MNI coordinates within the parietal cortex (bilateral IPS and SPL) for each individual participant. The objective of the ROI analysis was to determine the mean percent signal change (a measure BOLD response) in each ROI during each of the three contrasts (numbers, faces and shapes), to gain a better understanding of brain activity changes in small defined areas of interests (ROIs) and then to compare trends of BOLD signal between control and patient participants.

3.3.1 Bilateral Intraparietal Sulcus

During the number contrast (numbers > shapes & faces) we observed increased activation in the bilateral (right and left) intraparietal sulcus (IPS), in both the control group and patients. To quantify BOLD signal response for each participant we ran a ROI analysis for the right IPS [32 -68 42] and left IPS [-32 -68 43] by creating a 5 mm sphere around the respective MNI coordinates. We then calculated the mean percent signal change for each ROI in the individual participants, indicated by their ID number: controls (1B, 2B, 3B, 4B, 5B, 6B, 7B, 8B, 9B, 10B, 11B and 12B) and patients (2A, 4A, 5A) in each of the three contrasts (numbers, faces and shapes). The results of the ROI analysis calculating mean percent signal change (BOLD response) in the bilateral IPS are shown in Figure 17. The control participants appear on the left end of the graph, while the patient participants appear on the right end divided by the blue dotted line. Each contrast is indicated by a different color: number contrast (numbers > faces & shapes) in red, face contrast (faces > numbers & shapes) in yellow, and shape contrast (shapes > numbers & faces) in green. The number contrast generally displayed positive percent signal change, representing activation, for both the right IPS (Figure 17A) and left IPS (Figure 17B). During the shape contrast, participants generally had negative BOLD percent signal, representing deactivation. Therefore, bilateral IPS was deactivated during the shape stimuli of the fMRI task. The face condition was highly variable among the participants, having both positive and negative percent signal change.

A one sample t-test was conducted to determine whether there was a significant difference between the mean percent signal change (average of the mean percent signal change) of the all controls and the individual percent signal change for each patient (2A, 4A, 5A) during the number contrast. The alpha value for the one sample t-test was set to 0.05 ($\alpha = 0.05$). The average mean percent signal change for the control group for the right IPS was 0.275661 %, and for the left IPS 0.260885 %. The results of the one sample t-test for the right IPS and left IPS are shown in Table 9 and Table 10 respectively. In the right IPS, patients 2A ($p = 0.000788$) and 4A ($p = 0.000468$) were found to have a significantly greater mean percent signal change than the control group, going against our initial predictions in which the patients would experience lower percent signal change (attenuated BOLD signal) in parietal cortex during the number contrast, when compared to the healthy controls. Patient 5A ($p = 0.012153$) had a significantly lower mean percent signal change, when compared to the control group, which aligned with our predictions. For the left IPS, patient 2A ($p = 0.000021$), again had a significantly greater mean percent signal change, while patients 4A ($p = 0.963569$) and 5A ($p = 0.187450$) had no significant difference.

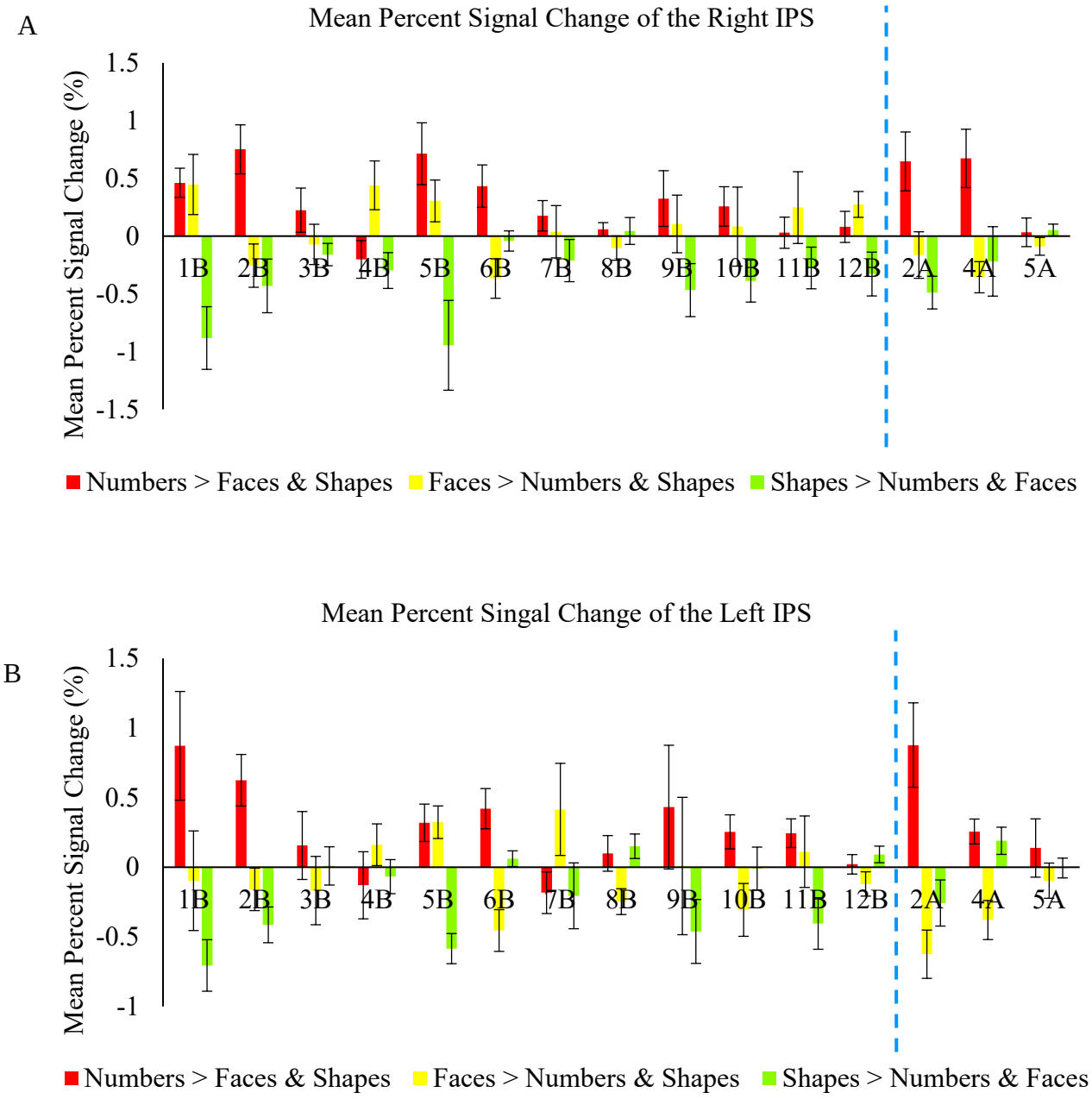

Figure 17: BOLD signal response in the bilateral IPS during each of the three contrasts (numbers, faces and shapes) for single participants. The bar graph above displays the mean percent signal change, a measure of BOLD signal, of the right IPS (A) and left IPS (B), during the number contrast (numbers > faces & shapes), face contrast (faces > numbers & shapes) and shape contrast (shapes > numbers & faces). Each participant is defined by the ID number, furthermore the participants are divided by the blue dotted line, with the control group are at the left side of the graph, while the patients are on the right end. The

standard deviation of the percent signal change for each contrast is indicated by the black error bars. The mean percent signal change was highly variable between the individual participants showing no difference between controls and patients.

Mean Percent Signal Change (%)		
Control Group	0.275661	Significance ($p < 0.05$)
Patient 2A	0.6467	Yes (p = 0.000788)
Patient 4A	0.6729	Yes (p = 0.000468)
Patient 5A	0.03298	Yes (p = 0.012153)

Table 9: Mean percent signal change of the right IPS for the control group, patient 2A, patient 4A, and patient 5A during the number contrast. Patients 2A and 4A had significantly greater mean percent signal change than the control group. While patient 5A had a significantly lower mean percent signal change when compared to the control group.

Mean Percent Signal Change (%)		
Control Group	0.260885	Significance ($p < 0.05$)
Patient 2A	0.8774	Yes (p = 0.000021)
Patient 4A	0.2568	No (p = 0.963569)
Patient 5A	0.138	No (p = 0.187450)

Table 10: Mean percent signal change of the left IPS for the control group, patient 2A, patient 4A, and patient 5A during the number contrast. Patient 2A had a significantly greater mean percent signal change than the control group. Patients 4A and 5A did not have a significant difference to that of the control group.

3.3.2 Bilateral Superior Parietal Lobule

During the number contrast (numbers > faces & shapes) activated clusters were localized in the bilateral superior parietal lobule (SPL). To quantify BOLD signal response for each participant, and ROI analysis was conducted for the right SPL [-32 -73 53] and left SPL [-32 -73 53] by calculating the mean percent signal change during each contrast (numbers, faces and shape), in order to determine levels of activation in the bilateral SPL and compare between the hydrocephalus patients and healthy controls. The results of the bilateral SPL ROI analysis are displayed in Figure 18. Participants had positive percent signal change in the number contrast the percentages had a high degree of variability, with no clear distinction in distribution between controls and patients. Interestingly, controls had higher percent signal in the left SPL (Figure 18A), when compared to the right SPL (Figure 18B) during the number contrast. Similar to the ROI analysis results for the IPS, the bilateral SPL displayed deactivation during the shape contrast, with negative percent signal change for most participants. A one sample t-test was conducted for each patient, in order to determine whether they had a significant difference to the average percent signal change of the control group for the bilateral SPL, the results are shown in Table 11 and Table 12. For the right SPL, patients 2A ($p = 0.013531$) and 4A ($p = 0.003162$) had a significantly greater mean percent signal change, while patient 5A ($p = 0.1422948$) did not have a significant difference when compared to the control group. In the left SPL patient 2A ($p = 0.014826$) had again had a significantly greater mean percent signal change, in contrast, patients 4A ($p = 0.531293$) and 5A ($p = 0.174020$) did not have a significant difference to that of the control group. For both the ROI results, for the bilateral IPS and SPL displayed a great deal of inter-participant variability among both the patients and controls, such that no definitive trends of BOLD signal could be concluded.

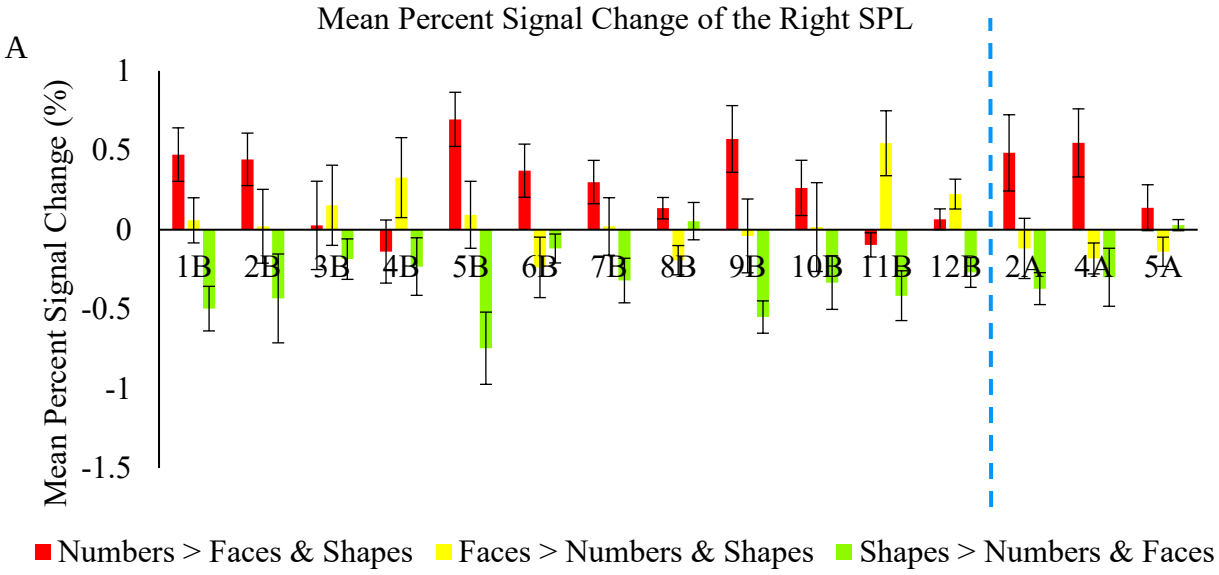

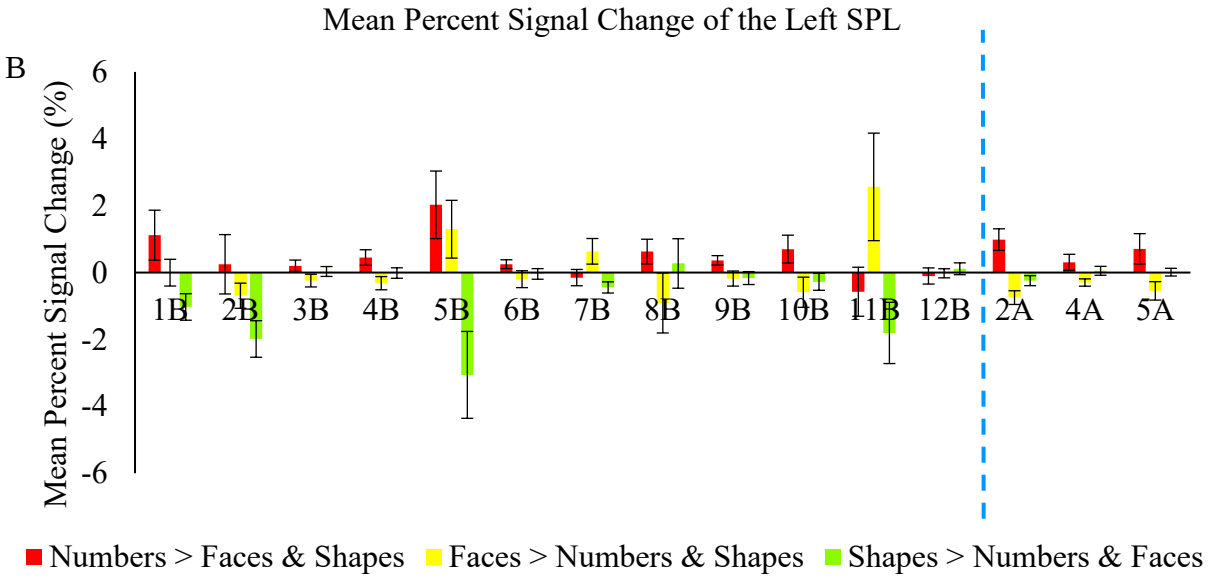

Figure 18: BOLD signal response in the bilateral SPL during each of the three contrasts (numbers, faces and shapes) for single participants. The bar graph above displays the mean percent signal change, a measure of BOLD signal, of the right SPL (A) and left SPL (B), during the number contrast (numbers > faces & shapes), face contrast (faces > numbers & shapes) and shape contrast (shapes > numbers & faces). Each participant is defined by the ID number, furthermore the participants are divided by the blue dotted line, with the control group are at the left side of the graph, while the patients are on the right end. The

standard deviation of the percent signal change for each contrast is indicated by the black error bars. The mean percent signal change was highly variable between the individual participants showing no difference between controls and patients.

Mean Percent Signal Change (%)		
Control Group	0.259350	Significance ($p < 0.05$)
Patient 2A	0.4837	Yes (p = 0.013531)
Patient 4A	0.5465	Yes (p = 0.003162)
Patient 5A	0.1386	No (p = 0.1422948)

Table 11: Mean percent signal change of the right SPL for the control group, patient 2A, patient 4A, and patient 5A during the number contrast. Patients 2A and 4A had a significantly greater mean percent signal change than the control group. Patient 5A did not have a significant difference to that of the control group.

Mean Percent Signal Change (%)		
Control Group	0.430667	Significance ($p < 0.05$)
Patient 2A	0.9854	Yes (p = 0.014826)
Patient 4A	0.3064	No (p = 0.531293)
Patient 5A	0.7101	No (p = 0.174020)

Table 12: Mean percent signal change of the left SPL for the control group, patient 2A, patient 4A, and patient 5A during the number contrast. Patient 2A had a significantly greater mean percent signal change than the control group. Patients 4A and 5A did not have a significant difference to that of the control group.

Chapter 4

4 Discussion and Conclusions

4.1 Discussion

The primary objective of the current study was to investigate how changes in posterior cortex development may lead to possible non-verbal learning deficits in school-aged children with treated infantile hydrocephalus. This was conducted as a case study, following the clinical history, behavioural assessments of three hydrocephalus patients (2A, 4A, 5A) who had all been diagnosed with and treated for infantile hydrocephalus before the age of two. The patients were compared to a group of healthy control children (n = 12). Furthermore, each of the participants underwent an fMRI number comparison task to localize parietal brain activity and compare BOLD signal activation between patients and controls.

The behavioural assessments (Beery VMI, WPPSI and WISC) all used standard scores which enabled across age comparison between the hydrocephalus patients and the healthy control group. Moreover, standard scores enabled us draw conclusions on level of performance (low, average, or high) for the hydrocephalus patients in relation to the mean standard scores. The hydrocephalus patients, 2A and 5A, had display trends of lower performance in the nonverbal assessments (Beery VMI, block design, arithmetic, and object assembly), which align with our stated hypothesis. Though, the hydrocephalus patients did display inter-subject differences, such that the patients did not share similar distributions in their test scores for the non-verbal and verbal assessments. For instance, patient 2A had average scores in the verbal assessments, information and vocabulary of the WISC; while displaying lower performance in all of their non-verbal assessments: Beery VMI, block design and arithmetic of the WISC. In contrast, patient 5A had low scores both their verbal and non-verbal assessments. On the WPPSI, patient 4A displayed average performance for information and block design, lower performance for vocabulary, and above average performance for object assembly in relation to the mean scaled score. Interestingly, patient 4A displayed above average performance in the Beery VMI subtests, having higher scores than the control group in VMI and visual perception subtests. While patients 2A and 5A had noticeably lower scores in all three subtests of the Beery VMI when compared to controls and mean standard score.

Differences surrounding the behavioural results among the hydrocephalus patients may be due to inter-participant variance; or perhaps differences in the pathological development of hydrocephalus among the individual patients, such as: prematurity, age of onset, etiology, or timing of treatment. Patient 2A behavioural scores had followed the predicted results, they had developed progressive hydrocephalus following the development of at 1 month of age. Patient 2A was subsequently monitored and serially tapped over the course of 3 months, followed by the insertion of a VP shunt at 4 months of age. Patient 5A displayed low scores in all of the assessments. Patient 5A was extremely preterm (born at 26 weeks of gestation) with a very low birth weight, both of which have been linked with abnormal brain development including cerebral volume reductions (Dorner et al., 2018; Eskandari et al., 2014; Thompson et al., 2007). Furthermore, patient 5A was diagnosed with a severe form of intraventricular hemorrhage (grades III and IV out of four) and meningitis, all of which have be associated with poor neurodevelopmental outcomes (Adams-Chapman et al., 2008; Anderson et al., 2003; Calisici et al., 2015; Dorner et al., 2018; Howe et al., 2016; Kohli-Lynch et al., 2017; Luu et al., 2009; Martis et al., 2019).

Due to patient 5A's young age at the time of diagnosis they were not shunted directly. They instead underwent endoscopic assisted pellucidotomy and underwent their VP shunt insertion after 5 months in the NICU. This late shunt insertion, after the time of diagnosis, may have resulted in prolonged ventricular dilatation and increased risk of neuroanatomical changes during patient 5A's first months of life, when an individual's brain is most plastic. Furthermore, the preoperative US of patient 5A (Figure 8A) showed the presence of periventricular cysts which has also been associated with poor neurodevelopmental outcomes (Cooper et al., 2016; Duerden et al., 2019; Imamura et al., 2013; Martinez-Biarge et al., 2019; Pappas et al., 2018; Smyser et al., 2013). Pathologic insults such as prolonged ventricle dilatation and white matter injury experienced on the developing brain can in turn lead to global cognitive impairments, as cited by multiple studies (Adams-Chapman et al., 2008; Anderson et al., 2003; Bhutta et al., 2002; Calisici et al., 2015; Dorner et al., 2019; Hannula-Sormunen et al., 2017; Howe et al., 2016; Lewis and Bendersky, 1989; Madzwamuse et al., 2015; Robinson, 2012). Coupled with their prematurity, severe hydrocephalus, periventricular cysts, neonatal infection, and late shunt insertion, patient 5A, unlike patients 4A and 2A, exhibited noticeably low scores in all of their behavioural assessments. Despite having overall low performance in each of the cognitive

batteries, patient 5A did display selective impairments, performing better in verbal tests over non-verbal tests, which parallels with prior studies involving hydrocephalus developmental outcomes showing hydrocephalic children have pronounced deficits in non-verbal cognition when compared to their verbal testing (Ayr et al., 2005; Barnes et al., 2002; Brookshire et al., 1995; Buckley et al., 2012, 2012; Dalen et al., 2006; Dennis et al., 1981b; Dorner et al., 2018, 2019; Fletcher et al., 1996c, 1996a; McAllister, 2012; McAllister et al., 1991b; Raybaud, 2017; Rourke, 1995; Rourke et al., 1990).

Interestingly patient 4A had displayed higher performance in non-verbal assessments, and low scores in the vocabulary subtest of WPPSI. Patient 4A was diagnosed with hydrocephalus secondary to Dandy Walker malformation at 3 weeks of age and was tapped twice both being shunted one week after their initial diagnosis. VP shunts are a permanent form of treatment by providing continual drainage of CSF fluid, thus making VP shunts a more effective form of treatment in reducing ventricular dilatation over serial taps which always require operative procedure to perform CSF drainage. A possible explanation for patient 4A's high scores in the cognitive assessment (Beery VMI, visual perception and motor coordination) may be due to their early shunt insertion which resulted in reduced ventricular dilatation and neuroanatomical changes. As ventricle dilatation progresses surrounding brain areas will experience compression, inflammation, edema, cell death resulting in a decrease in cortical thickness in a process known as cortical mantle thinning. Multiple studies have linked extent of ventricular dilatation with neuroanatomical changes which may in term result in neurodevelopmental deficits in childhood (Di Rocco et al., 2006; Rubin et al., 1976, 2008; Rubin and Hochwald, 1983; Venkataramana and Mukundan, 2011). VP shunt insertion can halt the progression of ventricular dilatation by reducing ventricle size and assist with cortical mantle recovery of affected areas. Radiographic studies investigating the effects of cortical thinning in infantile hydrocephalus have correlated clinical improvements in neurocognitive functions to recovery of cortical thickness in various brain areas (Rubin et al., 1976; Rubin and Hochwald, 1983; Venkataramana and Mukundan, 2011a), such that, brain areas that underwent cortical thinning during ventricular dilatation may regain thickness and restore functional outputs of the affected areas (Rubin et al., 1976, 2008; Rubin and Hochwald, 1983; Venkataramana and Mukundan, 2011b). Rubin et al., postulate that the recovery of cortical thickness is a compensatory mechanism and not a replacement of cortical areas that were lost. Furthermore, restoration of cortical thickness is only possible to a given

point after which damage and thinning become irreversible, such that, patients that early permanent CSF diversion such as VP shunts will have a better prognosis, like in the case of patient 4A.

Prolonged ventricular dilatation can result in permanent pathological reorganization of affected areas, that can lead to developmental deficits in their respective functional outputs, as seen in the posterior cortex. Less susceptible brain areas, such as the anterior cortex, will experience less damage and increase chance of recovery. This may be a possible explanation as to selective cognitive deficits in children with hydrocephalus, as seen in patients 2A and 5A. Despite having severe ventricular dilatation (Figure 7), patient 4A was shunted twice shortly after their initial diagnosis and was shunted only one week afterwards, and therefore never had large volume of CSF for long periods of time, preventing prolonged compression of their posterior cortex. Moreover, cortical areas associated with motor visual integration in patient 4A, such as the occipital cortex and parietal cortex may have had recovered cortical thickness and consequently normal outcomes in behavioural assessments for these regions. Having the degree of ventricular dilatation as a predictive model of neurodevelopmental outcomes should be further investigated using novel medical imaging utilities such as 3D US (Kishimoto et al., 2013, 2018; Qiu et al., 2013), in order to acquire acute ventricle size and volume and relate them to behavioural assessments.

Neurodevelopmental outcomes of children, whether healthy or patients, is a complicated process that can be influenced by multiple factors including: preterm birth, neurological conditions, as well as various social factors such as maternal education, single vs. two parent families, SES, familial support, and upbringing environment all work intermittently in playing a role in cognitive outcomes (Benavente-Fernández et al., 2019; Lodha et al., 2018; Ritzema et al., 2018). In the case of our patients (Table 2), patient 5A who had very low behavioural performance had the lowest maternal education and SES score, and was also was the only patient to have been from a single parent family, all of which have been associated with cognitive impairments during childhood (Calisici et al., 2015; Dorner et al., 2019; Lodha et al., 2018). Child resilience may also play a factor in the improved outcomes of patient 4A, who despite having Dandy Walker malformation with hydrocephalus at such a young age, had overcome their predicted disabilities, performing better than controls in some of the behavioural assessments (Beery VMI). Resilience

is defined as one's ability overcome a particular calamity, such as a medical condition (Bayat, 2007; Masten, 2018; Ritzema et al., 2018). Children overcoming expected disabilities and their general capacity to adapt to their given condition, is an extraordinary aspect of neurodevelopment one that should be acknowledged and trusted. Factors helping resilience, go beyond SES, but rather are a part of the supportive environment a child is brought up in. Familial support can work as a protective mechanism that can foster resilience, optimism, and acceptance, of a child's unique strengths and weaknesses (Bayat, 2007; Masten, 2018; Peer and Hillman, 2014).

To study the functional development of the posterior cortex, specifically the parietal lobe, we conducted an fMRI comparison task. During the number condition, both the controls and patients had activated clusters in parietal brain areas (bilateral IPS and SPL) associated with numeracy (Ansari, 2008; Ansari et al., 2005; Arsalidou et al., 2018; Cantlon et al., 2006; Dehaene et al., 2003; Emerson and Cantlon, 2012; Grabner et al., 2007; Matejko et al., 2018). An ROI analysis was performed to measure BOLD signal response for individual participants during each of the conditions (numbers, shapes & faces) for areas within the parietal cortex. Patients (2A, 4A) did not display attenuated BOLD signal when compared to healthy controls, and no difference was found in the distribution of percent signal change, as there was high degree of variability in BOLD signal between the participants. The patients had varying results that did not entirely align with our initial predictions. Possible explanations for this may be due to age related differences and brain signal variability among participants that come as a result of physiological responses such as heart rate or breathing (Grady and Garrett, 2018). Further research and analysis, with larger sample size, will be required to enable use to make more decisive inferences and explore the effects ventricular dilatation has on neuroanatomical functional development of the parietal cortex.

4.2 Limitations and Future Directions

In fMRI studies, recruitment and training can be challenging for pediatric patient participants. This caveat often leads to many fMRI studies being greatly underpowered by having small sample sizes. By having low study power, we cannot draw definitive conclusions with only fMRI data, since neuroimaging studies often require a large number of subjects and multiple statistical tests in order to determine significant differences among different testing groups. To overcome this, we utilized normed behavioural assessments, with individual fMRI measures to observe changes in functional brain activity in relation to the normalized behavioural scores of the individual patients with healthy controls. As recommended by Danckert and colleagues (Danckert and Mirsattarri, 2012) for single subject fMRI analysis we had a specific research hypothesis prior to scanning, with a brain areas of interest. Furthermore, we used an fMRI task based on the literature surrounding numerical processing and parietal cortex activation (Ansari, 2008; Cantlon et al., 2006; Emerson and Cantlon, 2012; Grabner et al., 2007), which allowed for robust bilateral activation.

In the future, data sharing and standard fMRI protocols should be considered, to improve study power while having baseline measures to assess acquired functional images data. Set ups such as databases with functional images with their respective task as well as information regarding activation patterns of interest could be useful for researchers globally. The creation of fMRI databases are still in their early stages with domains such as OpenfMRI, COINS, OASIS, and neurosyth (COINS: Collaborative Informatics and Neuroimaging Suite; Neurosynth; OpenfMRI; Marcus et al., 2007); taking the forefront in building functional image repositories of both healthy and clinical populations to assist in improving the understanding of neuronal processes during task presentation in fMRI. fMRI databases will help lay the foundation for normed fMRI measures that can be used in a similar manner as normed behavioural data. Such efforts will help broaden the study of functional neuroanatomical development in pediatric patients' populations.

For the ROI analysis, we found that percent BOLD signal change was highly variable among all participants. In the future, we could investigate patterns of activation in multiple brain areas through studying neuronal networks that are associated with a given cognitive domain such as numeracy, since the areas of the cortex never function alone but rather work intermittently in relation to one another. This would be more indicative as to what is actually occurring while a

participant is performing a given cognitive task, as well as provide better insight into neuronal organizational change in the posterior cortex. A useful modality to measure such relationships would be through measures of functional connectivity through resting state fMRI. Functional connectivity is the measurement of the changes in activation of between different brain regions over time, in order to determine their functional relationships (Brouwer et al., 2016). This can be measured using a correlation coefficient which ascertains the degree to which two variables' or in this case two regions' amount of activation are associated with one another, on a scale of -1.0 to + 1.0. We could take these measures of functional connectivity in known networks associated with non-verbal learning such as the frontoparietal network and relate them to performance in math tests (Emerson and Cantlon, 2012); in a correlation analysis between functional connectivity in the parietal cortex and non-verbal test scores as well as number of correct responses or reaction time during the fMRI task. A correlation analysis would enable us to determine whether functional connectivity can be used as a predictive measure of behavioural performance. Larger sample size will be required to conduct such analyses (Aggarwal and Ranganathan, 2016). With larger study size, we can also categorize the hydrocephalus patients into different sub-groups such as preterm and term births, ventricle volume prior shunt insertion, age of onset, and underlining cause of hydrocephalus. Classifying patients may assist in providing a better understanding of the neurodevelopment of hydrocephalus patients, while help explain behavioural differences among patients, as seen with patient 4A.

4.3 Conclusions

The objective for the current case study, was to investigative the behavioural outcomes of school-aged children with treated infantile hydrocephalus, specifically studying whether pathological anomalies in neuroanatomical development will lead to cognitive deficits in the functional outputs of those affected areas. We had hypothesized that, changes in posterior cortex development can be linked to non-verbal deficits. Particularly, we explored visuospatial and math skills in 3 patients as well as parietal cortex activity during an fMRI comparison task involving numbers. The behavioural assessments as well as the results of the ROI analysis displayed inter-participant variability among the individual patients, that did not align with our initial predictions. We found that clinical variables such as prematurity, age of onset, etiology, and timing of treatment, as well as SES factors, may influence the pathophysiology of infantile hydrocephalus and subsequently the neurodevelopmental outcomes experienced during childhood. The methodology as well as the findings of this case study offers insights for future research in utilizing fMRI alongside behavioural assessments for pediatric patient populations.

References

About Your Ventriculoperitoneal (VP) Shunt Surgery for Pediatric Patients *Memorial Sloan Kettering Cancer Center*. Available at: https://www.mskcc.org/cancer-care/patient-education/pediatric-ventriculoperitoneal-shunt-surgery [Accessed April 22, 2019].

Adams-Chapman, I., Hansen, N. I., Stoll, B. J., and Higgins, R. (2008). Neurodevelopmental Outcome of Extremely Low Birth Weight Infants With Posthemorrhagic Hydrocephalus Requiring Shunt Insertion. *Pediatrics* 121, e1167–e1177. doi:10.1542/peds.2007-0423.

Agarwal, N., Shukla, R. M., Agarwal, D., Gupta, K., Luthra, R., Gupta, J., et al. (2017). Pediatric Ventriculoperitoneal Shunts and their Complications: An Analysis. *J Indian Assoc Pediatr Surg* 22, 155–157. doi:10.4103/0971-9261.207624.

Aggarwal, R., and Ranganathan, P. (2016). Common pitfalls in statistical analysis: The use of correlation techniques. *Perspect Clin Res* 7, 187–190. doi:10.4103/2229-3485.192046.

Andersen, R. A. (2011). "Inferior Parietal Lobule Function in Spatial Perception and Visuomotor Integration," in *Comprehensive Physiology*, ed. R. Terjung (Hoboken, NJ, USA: John Wiley & Sons, Inc.), cp010512. doi:10.1002/cphy.cp010512.

Anderson, P., Doyle, L. W., and Group, and the V. I. C. S. (2003). Neurobehavioral Outcomes of School-age Children Born Extremely Low Birth Weight or Very Preterm in the 1990s. *JAMA* 289, 3264–3272. doi:10.1001/jama.289.24.3264.

Ansari, D. (2008). Effects of development and enculturation on number representation in the brain. *Nat. Rev. Neurosci.* 9, 278–291. doi:10.1038/nrn2334.

Ansari, D., Garcia, N., Lucas, E., Hamon, K., and Dhital, B. (2005). Neural correlates of symbolic number processing in children and adults. *Neuroreport* 16, 1769–1773. doi:10.1097/01.wnr.0000183905.23396.f1.

Arbabshirani, M. R., Plis, S., Sui, J., and Calhoun, V. D. (2017). Single subject prediction of brain disorders in neuroimaging: Promises and pitfalls. *NeuroImage* 145, 137–165. doi:10.1016/j.neuroimage.2016.02.079.

Armstrong, D., Halliday, W., Hawkins, C., and Takashima, S. eds. (2007). "Malformations," in *Pediatric Neuropathology: A Text-Atlas* (Tokyo: Springer Japan), 13–71. doi:10.1007/978-4-431-49898-8_2.

Arsalidou, M., Pawliw-Levac, M., Sadeghi, M., and Pascual-Leone, J. (2018). Brain areas associated with numbers and calculations in children: Meta-analyses of fMRI studies. *Developmental Cognitive Neuroscience* 30, 239–250. doi:10.1016/j.dcn.2017.08.002.

Aschoff, A., Kremer, P., Hashemi, B., and Kunze, S. (1999). The scientific history of hydrocephalus and its treatment. *Neurosurg Rev* 22, 67–93; discussion 94-95.

Ayr, L. K., Yeates, K. O., and Enrile, B. G. (2005). Arithmetic skills and their cognitive correlates in children with acquired and congenital brain disorder. *Journal of the International Neuropsychological Society* 11, 249–262. doi:10.1017/S1355617705050307.

Barnes, M. A., Pengelly, S., Dennis, M., Wilkinson, M., Rogers, T., and Faulkner, H. (2002). Mathematics skills in good readers with hydrocephalus. *J Int Neuropsychol Soc* 8, 72–82.

Basagni, B., Errante, A., Pinardi, C., De Gaetano, K., Crisi, G., De Tanti, A., et al. (2019). Rehabilitation of unilateral spatial neglect: A combined behavioral and fMRI single-case study. *Neuropsychology* 33, 343–357. doi:10.1037/neu0000523.

Battal, B., Kocaoglu, M., Bulakbasi, N., Husmen, G., Tuba Sanal, H., and Tayfun, C. (2011). Cerebrospinal fluid flow imaging by using phase-contrast MR technique. *Br J Radiol* 84, 758–765. doi:10.1259/bjr/66206791.

Bayat, M. (2007). Evidence of resilience in families of children with autism. *Journal of Intellectual Disability Research* 51, 702–714. doi:10.1111/j.1365-2788.2007.00960.x.

Beery, K. E., Beery, N. A., and PsychCorp (Firm) (2010). *Beery VMI. The Beery-Buktenica developmental test of visual-motor integration with supplemental developmental tests of visual perception and motor coordination: and, stepping stones age norms from birth to age six.*

Benavente-Fernández, I., Synnes, A., Grunau, R. E., Chau, V., Ramraj, C., Glass, T., et al. (2019). Association of Socioeconomic Status and Brain Injury With Neurodevelopmental Outcomes of Very Preterm Children. *JAMA Netw Open* 2, e192914–e192914. doi:10.1001/jamanetworkopen.2019.2914.

Bhutta, A. T., Cleves, M. A., Casey, P. H., Cradock, M. M., and Anand, K. J. S. (2002). Cognitive and Behavioral Outcomes of School-Aged Children Who Were Born Preterm: A Meta-analysis. *JAMA* 288, 728–737. doi:10.1001/jama.288.6.728.

Bigio, M. R. D. (2010). Neuropathology and structural changes in hydrocephalus. *Developmental Disabilities Research Reviews* 16, 16–22. doi:10.1002/ddrr.94.

Boklan, J. (2006). Little patients, losing patience: pediatric cancer drug development. *Mol Cancer Ther* 5, 1905–1908. doi:10.1158/1535-7163.MCT-06-0179.

Bolk, J., Padilla, N., Forsman, L., Broström, L., Hellgren, K., and Åden, U. (2018). Visual–motor integration and fine motor skills at 6½ years of age and associations with neonatal brain volumes in children born extremely preterm in Sweden: a population-based cohort study. *BMJ Open* 8, e020478. doi:10.1136/bmjopen-2017-020478.

Brodmann's Interactive Atlas Available at: http://www.fmriconsulting.com/brodmann/Introduction.html [Accessed July 9, 2019].

Brookes Publishing: Number Sense Screener™ (NSS™) Set, K–1, Research Edition Available at: http://products.brookespublishing.com/Number-Sense-Screener-NSS-Set-K1-Research-Edition-P469.aspx [Accessed April 12, 2018].

Brooks, M. E., and Pui, S. Y. (2010). Are individual differences in numeracy unique from general mental ability? A closer look at a common measure of numeracy. *Individual Differences Research* 8, 257–265.

Brookshire, B. L., Fletcher, J. M., Bohan, T. P., Landry, S. H., Davidson, K. C., and Francis, D. J. (1995). Verbal and Nonverbal Skill Discrepancies in Children with Hydrocephalus: A Five-Year Longitudinal Follow-Up 1. *Journal of Pediatric Psychology* 20, 785–800. doi:10.1093/jpepsy/20.6.785.

Brouwer, A. J., Stam, C. van, Venema, M. U., Koopman, C., Groenendaal, F., and Vries, L. S. de (2012). Cognitive and Neurological Outcome at the Age of 5–8 Years of Preterm Infants with Post-Hemorrhagic Ventricular Dilatation Requiring Neurosurgical Intervention. *NEO* 101, 210–216. doi:10.1159/000331797.

Brouwer, M. J., de Vries, L. S., Kersbergen, K. J., van der Aa, N. E., Brouwer, A. J., Viergever, M. A., et al. (2016). Effects of Posthemorrhagic Ventricular Dilatation in the Preterm Infant on Brain Volumes and White Matter Diffusion Variables at Term-Equivalent Age. *The Journal of Pediatrics* 168, 41-49.e1. doi:10.1016/j.jpeds.2015.09.083.

Brouwer, M. J., Vries, L. S. D., Pistorius, L., Rademaker, K. J., Groenendaal, F., and Benders, M. J. (2010). Ultrasound measurements of the lateral ventricles in neonates: why, how and when? A systematic review. *Acta Paediatrica* 99, 1298–1306. doi:10.1111/j.1651-2227.2010.01830.x.

Buckley, R. T., Yuan, W., Mangano, F. T., Phillips, J. M., Powell, S., McKinstry, R. C., et al. (2012). Longitudinal comparison of diffusion tensor imaging parameters and neuropsychological measures following endoscopic third ventriculostomy for hydrocephalus: Case report. *Journal of Neurosurgery: Pediatrics* 9, 630–635. doi:10.3171/2012.2.PEDS11331.

Calisici, E., Eras, Z., Oncel, M. Y., Oguz, S. S., Gokce, İ. K., and Dilmen, U. (2015). Neurodevelopmental outcomes of premature infants with severe intraventricular hemorrhage. *The Journal of Maternal-Fetal & Neonatal Medicine* 28, 2115–2120. doi:10.3109/14767058.2014.979783.

Cantlon, J. F., Brannon, E. M., Carter, E. J., and Pelphrey, K. A. (2006). Functional Imaging of Numerical Processing in Adults and 4-y-Old Children. *PLoS Biol* 4. doi:10.1371/journal.pbio.0040125.

Cavalheiro, S., da Costa, M. D. S., Mendonça, J. N., Dastoli, P. A., Suriano, I. C., Barbosa, M. M., et al. (2017). Antenatal management of fetal neurosurgical diseases. *Childs Nerv Syst* 33, 1125–1141. doi:10.1007/s00381-017-3442-x.

Cerebrospinal fluid (2019). *Wikipedia*. Available at: https://en.wikipedia.org/w/index.php?title=Cerebrospinal_fluid&oldid=878834798 [Accessed January 23, 2019].

Chin-Lun Hung, G., Hahn, J., Alamiri, B., Buka, S. L., Goldstein, J. M., Laird, N., et al. (2015). Socioeconomic disadvantage and neural development from infancy through early childhood. *Int J Epidemiol* 44, 1889–1899. doi:10.1093/ije/dyv303.

Cinalli, G., Maixner, W. J., and Sainte-Rose, C. (2004). *Pediatric Hydrocephalus*. Springer.

Cirino, P., Chin, C., Sevcik, R., Wolf, M., Lovett, M., and Morris, R. (2002). Measuring Socioeconomic Status: Reliability and Preliminary Validity for Different Approaches. *Assessment* 9, 145–155. doi:10.1177/10791102009002005.

COINS: Collaborative Informatics and Neuroimaging Suite Available at: https://coins.trendscenter.org/ [Accessed June 10, 2019].

Comerford, M., Lourens, S., Liangpunsakul, S., Chalasani, N. P., Sanyal, A. J., Shah, V. H., et al. (2017). Challenges in Patient Enrollment and Retention in Clinical Studies for Alcoholic Hepatitis: Experience of the TREAT Consortium. *Alcohol. Clin. Exp. Res.* 41, 2000–2006. doi:10.1111/acer.13515.

Cooper, S., Bar-Yosef, O., Berkenstadt, M., Hoffmann, C., Achiron, R., and Katorza, E. (2016). Prenatal Evaluation, Imaging Features, and Neurodevelopmental Outcome of Prenatally Diagnosed Periventricular Pseudocysts. *AJNR Am J Neuroradiol* 37, 2382–2388. doi:10.3174/ajnr.A4916.

Dalen, K., Bruarøy, S., Wentzel-Larsen, T., Nygaard, M., and Laegreid, L. M. (2006). Non-Verbal Learning Disabilities in Children with Infantile Hydrocephalus, Aged 4 - 7 Years: A Population-Based, Controlled Study. *Neuropediatrics* 37, 1–5. doi:10.1055/s-2006-923839.

Dalrymple, K.A., Gomez, J., and Duchaine, B. The Dartmouth Database of Children's Faces: Acquisition and validation of a new face stimulus set.

Danckert, J., and Mirsattarri, S. M. (2012). Neuroimaging of Single Cases: Benefits and Pitfalls. *Neuroimaging - Cognitive and Clinical Neuroscience*. doi:10.5772/22983.

de Bertoldi, F., Finos, L., Maieron, M., Weis, L., Campanella, M., Ius, T., et al. (2015). Improving the reliability of single-subject fMRI by weighting intra-run variability. *NeuroImage* 114, 287–293. doi:10.1016/j.neuroimage.2015.03.076.

De Vega, M., Denis, M., Intons-Peterson, M. J., Johnson-Laird, P. N., and Marschark, M. (1996). *Models of Visuospatial Cognition*. Cary, UNITED STATES: Oxford University Press, Incorporated Available at: http://ebookcentral.proquest.com/lib/west/detail.action?docID=272312 [Accessed June 23, 2019].

Dehaene, S., Piazza, M., Pinel, P., and Cohen, L. (2003). Three Parietal Circuits for Number Processing. *Cognitive Neuropsychology* 20, 487–506. doi:10.1080/02643290244000239.

Del Bigio, M. R. (1993). Neuropathological changes caused by hydrocephalus. *Acta Neuropathol.* 85, 573–585.

Denhoff, E. R., Milliren, C. E., de Ferranti, S. D., Steltz, S. K., and Osganian, S. K. (2015). Factors Associated with Clinical Research Recruitment in a Pediatric Academic Medical Center--A Web-Based Survey. *PLoS ONE* 10, e0140768. doi:10.1371/journal.pone.0140768.

Dennis, M., Fitz, C. R., Netley, C. T., Sugar, J., Harwood-Nash, D. C. F., Hendrick, E. B., et al. (1981a). The Intelligence of Hydrocephalic Children. *Arch Neurol* 38, 607–615. doi:10.1001/archneur.1981.00510100035004.

Dennis, M., Fitz, C. R., Netley, C. T., Sugar, J., Harwood-Nash, D. C. F., Hendrick, E. B., et al. (1981b). The Intelligence of Hydrocephalic Children. *Arch Neurol* 38, 607–615. doi:10.1001/archneur.1981.00510100035004.

Deoni, S. C. L., Mercure, E., Blasi, A., Gasston, D., Thomson, A., Johnson, M., et al. (2011). Mapping Infant Brain Myelination with Magnetic Resonance Imaging. *J. Neurosci.* 31, 784–791. doi:10.1523/JNEUROSCI.2106-10.2011.

DeSilva, J., and Lesnik, J. (2008). Brain size at birth throughout human evolution: a new method for estimating neonatal brain size in hominins. *J Hum Evol* 55. doi:10.1016/j.jhevol.2008.07.008.

Di Rocco, C., Massimi, L., and Tamburrini, G. (2006). Shunts vs endoscopic third ventriculostomy in infants: are there different types and/or rates of complications? *Childs Nerv Syst* 22, 1573–1589. doi:10.1007/s00381-006-0194-4.

Dorner, R. A., Burton, V. J., Allen, M. C., Robinson, S., and Soares, B. P. (2018). Preterm neuroimaging and neurodevelopmental outcome: a focus on intraventricular hemorrhage, post-hemorrhagic hydrocephalus, and associated brain injury. *Journal of Perinatology* 38, 1431. doi:10.1038/s41372-018-0209-5.

Dorner, R. A., Soares, B. P., Robinson, S., Allen, M. C., Perin, J., and Burton, V. J. (2019). The Relationship Between Clinical Imaging and Neurobehavioral Assessment in Posthemorrhagic Ventricular Dilation of Prematurity. *Front. Physiol.* 10. doi:10.3389/fphys.2019.00064.

Dubois, J., and Adolphs, R. (2016). Building a Science of Individual Differences from fMRI. *Trends in Cognitive Sciences* 20, 425–443. doi:10.1016/j.tics.2016.03.014.

Duerden, E. G., Halani, S., Ng, K., Guo, T., Foong, J., Glass, T. J. A., et al. (2019). White matter injury predicts disrupted functional connectivity and microstructure in very preterm born neonates. *NeuroImage: Clinical* 21, 101596. doi:10.1016/j.nicl.2018.11.006.

Edes, A. E., Kozak, L. R., Magyar, M., Zsombok, T., Kokonyei, G., Bagdy, G., et al. (2017). Spontaneous migraine attack causes alterations in default mode network connectivity: a resting-state fMRI case report. *BMC Research Notes* 10, 1–5.

Ekstrom, A. (2010). How and when the fMRI BOLD signal relates to underlying neural activity: The danger in dissociation. *Brain Res Rev* 62, 233–244. doi:10.1016/j.brainresrev.2009.12.004.

Emerson, R. W., and Cantlon, J. F. (2012). Early math achievement and functional connectivity in the fronto-parietal network. *Developmental Cognitive Neuroscience* 2, S139–S151. doi:10.1016/j.dcn.2011.11.003.

E-Prime 2.0 Psychology Software Tools, Inc. Available at: https://pstnet.com/.

Eskandari, R., Abdullah, O., Mason, C., Lloyd, K. E., Oeschle, A. N., and McAllister, J. P. (2014). Differential vulnerability of white matter structures to experimental infantile hydrocephalus detected by diffusion tensor imaging. *Childs Nerv Syst* 30, 1651–1661. doi:10.1007/s00381-014-2500-x.

Evans, A. C. (2006). The NIH MRI study of normal brain development. *NeuroImage* 30, 184–202. doi:10.1016/j.neuroimage.2005.09.068.

Ferrari, A., Montello, M., Budd, T., and Bleyer, A. (2008). The challenges of clinical trials for adolescents and young adults with cancer. *Pediatric Blood & Cancer* 50, 1101–1104. doi:10.1002/pbc.21459.

Fletcher, J. M., Bohan, T. P., Brandt, M. E., Brookshire, B. L., Beaver, S. R., Francis, D. J., et al. (1992). Cerebral white matter and cognition in hydrocephalic children. *Arch. Neurol.* 49, 818–824.

Fletcher, J. M., Bohan, T. P., Brandt, M. E., Kramer, L. A., Brookshire, B. L., Thorstad, K., et al. (1996a). Morphometric evaluation of the hydrocephalic brain: relationships with cognitive development. *Childs Nerv Syst* 12, 192–199.

Fletcher, J. M., McCauley, S. R., Brandt, M. E., Bohan, T. P., Kramer, L. A., Francis, D. J., et al. (1996b). Regional Brain Tissue Composition in Children With Hydrocephalus: Relationships With Cognitive Development. *Arch Neurol* 53, 549–557. doi:10.1001/archneur.1996.00550060093022.

Fletcher, J. M., McCauley, S. R., Brandt, M. E., Bohan, T. P., Kramer, L. A., Francis, D. J., et al. (1996c). Regional Brain Tissue Composition in Children With Hydrocephalus: Relationships With Cognitive Development. *Arch Neurol* 53, 549–557. doi:10.1001/archneur.1996.00550060093022.

Fonov, V., Evans, A. C., Botteron, K., Almli, C. R., McKinstry, R. C., and Collins, D. L. (2011). Unbiased average age-appropriate atlases for pediatric studies. *Neuroimage* 54, 313–327. doi:10.1016/j.neuroimage.2010.07.033.

Fulmer, B. B., Grabb, P. A., Oakes, W. J., and Mapstone, T. B. (2000). Neonatal Ventriculosubgaleal Shunts. *Neurosurgery* 47, 80–84. doi:10.1097/00006123-200007000-00018.

Gaillard, F. Obstructive hydrocephalus | Radiology Reference Article | Radiopaedia.org. *Radiopaedia*. Available at: https://radiopaedia.org/articles/obstructive-hydrocephalus [Accessed August 7, 2019].

Gammal, T., Allen, M., Brooks, B., and Mark, E. (1987). MR evaluation of hydrocephalus. *American Journal of Roentgenology* 149, 807–813. doi:10.2214/ajr.149.4.807.

Glickman, S. W., Anstrom, K. J., Lin, L., Chandra, A., Laskowitz, D. T., Woods, C. W., et al. (2008). Challenges in Enrollment of Minority, Pediatric, and Geriatric Patients in Emergency and Acute Care Clinical Research. *Annals of Emergency Medicine* 51, 775-780.e3. doi:10.1016/j.annemergmed.2007.11.002.

Gorgolewski, K. J., Auer, T., Calhoun, V. D., Craddock, R. C., Das, S., Duff, E. P., et al. (2016). The brain imaging data structure, a format for organizing and describing outputs of neuroimaging experiments. *Scientific Data* 3, 160044. doi:10.1038/sdata.2016.44.

Grabner, R. H., Ansari, D., Reishofer, G., Stern, E., Ebner, F., and Neuper, C. (2007). Individual differences in mathematical competence predict parietal brain activation during mental calculation. *Neuroimage* 38, 346–356. doi:10.1016/j.neuroimage.2007.07.041.

Grady, C. L., and Garrett, D. D. (2018). Brain signal variability is modulated as a function of internal and external demand in younger and older adults. *NeuroImage* 169, 510–523. doi:10.1016/j.neuroimage.2017.12.031.

Greve, D. N., and Fischl, B. (2009). Accurate and robust brain image alignment using boundary-based registration. *NeuroImage* 48, 63–72. doi:10.1016/j.neuroimage.2009.06.060.

Halm, B., Leone, T., Chaudoin, L., McKinley, K., Ruzal-Shapiro, C., Franke, A., et al. (2018). Evaluation of Ventricle Size Measurements in Infants by Pediatric Emergency Medicine Physicians. *Pediatric Emergency Care* Publish Ahead of Print. doi:10.1097/PEC.0000000000001497.

Hannula-Sormunen, M. M., Nanu, C. E., Laakkonen, E., Munck, P., Kiuru, N., and Lehtonen, L. (2017). Early mathematical skill profiles of prematurely and full-term born children. *Learning and Individual Differences* 55, 108–119. doi:10.1016/j.lindif.2017.03.004.

Holwerda, J. C., Van Braeckel, K. N. J. A., Roze, E., Hoving, E. W., Maathuis, C. G. B., Brouwer, O. F., et al. (2016). Functional outcome at school age of neonatal post-hemorrhagic ventricular dilatation. *Early Human Development* 96, 15–20. doi:10.1016/j.earlhumdev.2016.02.005.

Howe, T.-H., Sheu, C.-F., Hsu, Y.-W., Wang, T.-N., and Wang, L.-W. (2016). Predicting neurodevelopmental outcomes at preschool age for children with very low birth weight. *Research in Developmental Disabilities* 48, 231–241. doi:10.1016/j.ridd.2015.11.003.

Huettel, S. A., Song, A. W., and McCarthy, G. (2014). *Functional magnetic resonance imaging*. Sinauer Associates, Inc., Publishers.

Hydrocephalus (2019). *Wikipedia*. Available at: https://en.wikipedia.org/w/index.php?title=Hydrocephalus&oldid=881990572 [Accessed February 13, 2019].

hydrocephalus | Definition of hydrocephalus in English by Oxford Dictionaries *Oxford Dictionaries | English*. Available at: https://en.oxforddictionaries.com/definition/hydrocephalus [Accessed January 23, 2019].

Hydrocephalus During Infancy | The Embryo Project Encyclopedia Available at: https://embryo.asu.edu/pages/hydrocephalus-during-infancy [Accessed April 12, 2018].

Imamura, T., Ariga, H., Kaneko, M., Watanabe, M., Shibukawa, Y., Fukuda, Y., et al. (2013). Neurodevelopmental outcomes of children with periventricular leukomalacia. *Pediatr Neonatol* 54, 367–372. doi:10.1016/j.pedneo.2013.04.006.

Iyengar, S. (2016). Case for fMRI data repositories. *PNAS* 113, 7699–7700. doi:10.1073/pnas.1608146113.

Kadam, R. A., Borde, S. U., Madas, S. A., Salvi, S. S., and Limaye, S. S. (2016). Challenges in recruitment and retention of clinical trial subjects. *Perspect Clin Res* 7, 137–143. doi:10.4103/2229-3485.184820.

Kahle, K. T., Kulkarni, A. V., Limbrick, D. D., and Warf, B. C. (2016). Hydrocephalus in children. *The Lancet* 387, 788–799. doi:10.1016/S0140-6736(15)60694-8.

Khan, O. H., Enno, T. L., and Del Bigio, M. R. (2006). Brain damage in neonatal rats following kaolin induction of hydrocephalus. *Experimental Neurology* 200, 311–320. doi:10.1016/j.expneurol.2006.02.113.

Kishimoto, J., de Ribaupierre, S., Lee, D. S. C., Mehta, R., St Lawrence, K., and Fenster, A. (2013). 3D ultrasound system to investigate intraventricular hemorrhage in preterm neonates. *Phys Med Biol* 58, 7513–7526. doi:10.1088/0031-9155/58/21/7513.

Kishimoto, J., Fenster, A., Lee, D. S. C., and de Ribaupierre, S. (2018). Quantitative 3-D head ultrasound measurements of ventricle volume to determine thresholds for preterm neonates requiring interventional therapies following posthemorrhagic ventricle dilatation. *J Med Imaging (Bellingham)* 5, 026001. doi:10.1117/1.JMI.5.2.026001.

Klingberg, T., Forssberg, H., and Westerberg, H. (2002). Increased Brain Activity in Frontal and Parietal Cortex Underlies the Development of Visuospatial Working Memory Capacity during Childhood. *Journal of Cognitive Neuroscience* 14, 1–10. doi:10.1162/089892902317205276.

Kohli-Lynch, M., Russell, N. J., Seale, A. C., Dangor, Z., Tann, C. J., Baker, C. J., et al. (2017). Neurodevelopmental Impairment in Children After Group B Streptococcal Disease

Worldwide: Systematic Review and Meta-analyses. *Clin Infect Dis* 65, S190–S199. doi:10.1093/cid/cix663.

Korsnes, M., Hugdahl, K., and Bjørnæs, H. (2009). An fMRI case study of visual memory in a patient with epilepsy: comparison before and after temporal lobe surgery. *Brain Structure and Function* 213, 457–462. doi:10.1007/s00429-009-0216-6.

Krause, M., Panteliadis, C. P., Hagel, C., Hirsch, F. W., Thome, U. H., Meixensberger, J., et al. (2017). Surgical Treatment for Neonatal Hydrocephalus: Catheter-Based Cerebrospinal Fluid Diversion or Endoscopic Intervention? *Open Journal of Modern Neurosurgery* 08, 30. doi:10.4236/ojmn.2018.81002.

Krause, M., Panteliadis, C. P., Hagel, C., Hirsch, F. W., Thome, U. H., Meixensberger, J., et al. (2018). Surgical Treatment for Neonatal Hydrocephalus: Catheter-Based Cerebrospinal Fluid Diversion or Endoscopic Intervention? *Open Journal of Modern Neurosurgery* 08, 30–45. doi:10.4236/ojmn.2018.81002.

Kulkarni, A. V., Donnelly, R., Mabbott, D. J., and Widjaja, E. (2015). Relationship between ventricular size, white matter injury, and neurocognition in children with stable, treated hydrocephalus. *Journal of Neurosurgery: Pediatrics* 16, 267–274. doi:10.3171/2015.1.PEDS14597.

Kulkarni, A. V., Donnelly, R., and Shams, I. (2011). Comparison of Hydrocephalus Outcome Questionnaire scores to neuropsychological test performance in school-aged children: Clinical article. *Journal of Neurosurgery: Pediatrics* 8, 396–401. doi:10.3171/2011.7.PEDS1179.

Lacadie, C. M., Fulbright, R. K., Constable, R. T., and Papademetris, X. (2008). More Accurate Talairach Coordinates for NeuroImaging using Nonlinear Registration. *Neuroimage* 42, 717–725. doi:10.1016/j.neuroimage.2008.04.240.

Lewis, M., and Bendersky, M. (1989). Cognitive and Motor Differences Among Low Birth Weight Infants: Impact of Intraventricular Hemorrhage, Medical Risk, and Social Class. *Pediatrics* 83, 187–192.

Lin, Z., Yu, B., Liang, Z., Chen, X., Liu, J., Chen, S., et al. (2009). [Role of Ommaya reservoir in the management of neonates with post-hemorrhagic hydrocephalus]. *Zhonghua Er Ke Za Zhi* 47, 140–145.

Lindquist, B., Persson, E.-K., Uvebrant, P., and Carlsson, G. (2008). Learning, memory and executive functions in children with hydrocephalus. *Acta Paediatrica* 97, 596–601. doi:10.1111/j.1651-2227.2008.00747.x.

Lodha, A., Lakhani, J., Ediger, K., Tang, S., Lodha, A., Gandhi, V., et al. (2018). Do preterm infants with a birth weight ≤1250 g born to single-parent families have poorer neurodevelopmental outcomes at age 3 than those born to two-parent families? *J Perinatol* 38, 900–907. doi:10.1038/s41372-018-0118-7.

Luu, T. M., Ment, L. R., Schneider, K. C., Katz, K. H., Allan, W. C., and Vohr, B. R. (2009). Lasting Effects of Preterm Birth and Neonatal Brain Hemorrhage at 12 Years of Age. *Pediatrics* 123, 1037–1044. doi:10.1542/peds.2008-1162.

Lv, H., Wang, Z., Tong, E., Williams, L. M., Zaharchuk, G., Zeineh, M., et al. (2018). Resting-State Functional MRI: Everything That Nonexperts Have Always Wanted to Know. *American Journal of Neuroradiology*. doi:10.3174/ajnr.A5527.

Madzwamuse, S. E., Baumann, N., Jaekel, J., Bartmann, P., and Wolke, D. (2015). Neuro-cognitive performance of very preterm or very low birth weight adults at 26 years. *Journal of Child Psychology and Psychiatry* 56, 857–864. doi:10.1111/jcpp.12358.

Magnetism *Questions and Answers in MRI*. Available at: http://mriquestions.com/does-boldbrain-activity.html [Accessed May 5, 2019].

Marcus, D. S., Wang, T. H., Parker, J., Csernansky, J. G., Morris, J. C., and Buckner, R. L. (2007). Open Access Series of Imaging Studies (OASIS): Cross-sectional MRI Data in Young, Middle Aged, Nondemented, and Demented Older Adults. *Journal of Cognitive Neuroscience* 19, 1498–1507. doi:10.1162/jocn.2007.19.9.1498.

Martinez-Biarge, M., Groenendaal, F., Kersbergen, K. J., Benders, M. J. N. L., Foti, F., van Haastert, I. C., et al. (2019). Neurodevelopmental Outcomes in Preterm Infants with White Matter Injury Using a New MRI Classification. *NEO*, 1–9. doi:10.1159/000499346.

Martis, J. M. S., Bok, L. A., Halbertsma, F. J. J., Straaten, H. L. M. van, Vries, L. S. de, and Groenendaal, F. (2019). Brain imaging can predict neurodevelopmental outcome of Group B streptococcal meningitis in neonates. *Acta Paediatrica* 108, 855–864. doi:10.1111/apa.14593.

Masten, A. S. (2018). Resilience Theory and Research on Children and Families: Past, Present, and Promise. *Journal of Family Theory & Review* 10, 12–31. doi:10.1111/jftr.12255.

Mataró, M., Junqué, C., Poca, M. A., and Sahuquillo, J. (2001). Neuropsychological Findings in Congenital and Acquired Childhood Hydrocephalus. *Neuropsychol Rev* 11, 169–178. doi:10.1023/A:1012904907249.

Matejko, A. A., and Ansari, D. (2019). The neural association between arithmetic and basic numerical processing depends on arithmetic problem size and not chronological age. *Developmental Cognitive Neuroscience* 37, 100653. doi:10.1016/j.dcn.2019.100653.

Matejko, A. A., Hutchison, J. E., and Ansari, D. (2018). Developmental specialization of the left intraparietal sulcus for symbolic ordinal processing. *Cortex*. doi:10.1016/j.cortex.2018.11.027.

Mazaika, P. Percent Signal Change for fMRI. 8.

McAllister, J. P. (2012). Pathophysiology of congenital and neonatal hydrocephalus. *Seminars in Fetal and Neonatal Medicine* 17, 285–294. doi:10.1016/j.siny.2012.06.004.

McAllister, J. P., Cohen, M. I., O'Mara, K. A., and Johnson, M. H. (1991a). Progression of experimental infantile hydrocephalus and effects of ventriculoperitoneal shunts: an analysis correlating magnetic resonance imaging with gross morphology. *Neurosurgery* 29, 329–340.

McAllister, J. P. I., Cohen, M. I. M. D., O'Mara, K. A. M. D., and Johnson, M. H. M. D. (1991b). Progression of Experimental Infantile Hydrocephalus and Effects of Ventriculoperitoneal Shunts: An Analysis Correlating Magnetic Resonance Imaging with Gross Morphology. *Neurosurgery* 29, 329–340.

McCarthy, P. (2019). *FSLeyes*. Zenodo doi:10.5281/zenodo.3258216.

Michelson, D., Ciafaloni, E., Ashwal, S., Lewis, E., Narayanaswami, P., Oskoui, M., et al. (2018). Evidence in focus: Nusinersen use in spinal muscular atrophy: Report of the Guideline Development, Dissemination, and Implementation Subcommittee of the American Academy of Neurology. *Neurology* 91, 923–933. doi:10.1212/WNL.0000000000006502.

Miedzińska, M., Hnatyszyn, G., Konefał, H., Hernicka-Stawiarska, M., Modrzejewska, M., Kabacińska, A., et al. (2012). [Meningitis and chosen complications of neonatal period in preterm neonates born to single or multiple pregnancies]. *Ginekol. Pol.* 83, 202–208.

Mock, J., Huber, S., Bloechle, J., Dietrich, J. F., Bahnmueller, J., Rennig, J., et al. (2018). Magnitude processing of symbolic and non-symbolic proportions: an fMRI study. *Behav Brain Funct* 14. doi:10.1186/s12993-018-0141-z.

Mohammad, M. H., and Diaz, R. J. (2017). Technical and anatomical aspects of endoscopically assisted septostomy in unilateral ventriculoperitoneal shunt placement for the management of isolated lateral ventricles. *Interdisciplinary Neurosurgery* 10, 32–36. doi:10.1016/j.inat.2017.05.003.

Mussolin, C., Mejias, S., and Noël, M.-P. (2010). Symbolic and nonsymbolic number comparison in children with and without dyscalculia. *Cognition* 115, 10–25. doi:10.1016/j.cognition.2009.10.006.

Nemmi, F., Bianchini, F., Piras, F., Péran, P., Palermo, L., Piccardi, L., et al. (2015). Finding my own way: an fMRI single case study of a subject with developmental topographical disorientation. *Neurocase* 21, 573–583. doi:10.1080/13554794.2014.960424.

Neurosynth Available at: http://neurosynth.org/ [Accessed June 10, 2019].

Obeid, R., Tabrizi, P. R., Mansoor, A., Cerrolaza, J. J., Chang, T., Penn, A. A., et al. (2019). Ventricular shape evaluation on early ultrasound predicts post-hemorrhagic hydrocephalus. *Pediatric Research* 85, 293. doi:10.1038/s41390-018-0252-0.

OpenfMRI Available at: https://openfmri.org/ [Accessed June 10, 2019].

Pan, P. (2018). Outcome Analysis of Ventriculoperitoneal Shunt Surgery in Pediatric Hydrocephalus. *J Pediatr Neurosci* 13, 176–181. doi:10.4103/jpn.JPN_29_18.

Pappas, A., Adams-Chapman, I., Shankaran, S., McDonald, S. A., Stoll, B. J., Laptook, A. R., et al. (2018). Neurodevelopmental and Behavioral Outcomes in Extremely Premature Neonates With Ventriculomegaly in the Absence of Periventricular-Intraventricular Hemorrhage. *JAMA Pediatr* 172, 32–42. doi:10.1001/jamapediatrics.2017.3545.

Patel, D. M., Tubbs, R. S., Pate, G., Johnston, J. M., and Blount, J. P. (2014). Fast-sequence MRI studies for surveillance imaging in pediatric hydrocephalus. *J Neurosurg Pediatr* 13, 440–447. doi:10.3171/2014.1.PEDS13447.

Pediatric Radiology Available at: https://www.med-ed.virginia.edu/courses/rad/peds/neuro_webpages/b15.html [Accessed December 29, 2017].

Peer, J. W., and Hillman, S. B. (2014). Stress and Resilience for Parents of Children With Intellectual and Developmental Disabilities: A Review of Key Factors and Recommendations for Practitioners. *Journal of Policy and Practice in Intellectual Disabilities* 11, 92–98. doi:10.1111/jppi.12072.

Physical Growth in Newborns - Topic Overview Available at: https://myhealth.alberta.ca:443/Health/pages/conditions.aspx?hwid=te6295 [Accessed April 28, 2019].

Pinchefsky, E. F., Accogli, A., Shevell, M. I., Saint-Martin, C., and Srour, M. (2019). Developmental outcomes in children with congenital cerebellar malformations. *Developmental Medicine & Child Neurology* 61, 350–358. doi:10.1111/dmcn.14059.

Pizoli, C. E., Shah, M. N., Snyder, A. Z., Shimony, J. S., Limbrick, D. D., Raichle, M. E., et al. (2011). Resting-state activity in development and maintenance of normal brain function. *PNAS* 108, 11638–11643. doi:10.1073/pnas.1109144108.

Principles of magnetic resonance imaging - 1 (2015). in *MRI Basic Principles and Applications* (John Wiley & Sons, Ltd), 26–38. doi:10.1002/9781119013068.ch4.

Qiu, W., Yuan, J., Kishimoto, J., Ukwatta, E., and Fenster, A. (2013). Lateral ventricle segmentation of 3D pre-term neonates US using convex optimization. *Med Image Comput Comput Assist Interv* 16, 559–566.

Radman, N., Mouthon, M., Pietro, M. D., Gaytanidis, C., Leemann, B., Abutalebi, J., et al. (2016). The Role of the Cognitive Control System in Recovery from Bilingual Aphasia: A Multiple Single-Case fMRI Study. *Neural Plasticity* 2016. Available at: https://doaj.org [Accessed May 20, 2019].

Raybaud, C. (2017). “Neuroimaging in Pediatric Hydrocephalus,” in *Textbook of Pediatric Neurosurgery*, eds. C. Di Rocco, D. Pang, and J. T. Rutka (Cham: Springer International Publishing), 1–111. doi:10.1007/978-3-319-31512-6_15-1.

Rekate, H. L. (2008). The definition and classification of hydrocephalus: a personal recommendation to stimulate debate. *Cerebrospinal Fluid Res* 5, 2. doi:10.1186/1743-8454-5-2.

Ritzema, A. M., Lach, L. M., Nicholas, D., and Sladeczek, I. E. (2018). A model of well-being for children with neurodevelopmental disorders: Parental perceptions of functioning, services, and support. *Child: Care, Health and Development* 44, 240–248. doi:10.1111/cch.12541.

Robinson, S. (2012). Neonatal posthemorrhagic hydrocephalus from prematurity: pathophysiology and current treatment concepts: A review. *Journal of neurosurgery. Pediatrics* 9. doi:10.3171/2011.12.PEDS11136.

Roland, J. L., Griffin, N., Hacker, C. D., Vellimana, A. K., Akbari, S. H., Shimony, J. S., et al. (2017). Resting-state functional magnetic resonance imaging for surgical planning in pediatric patients: a preliminary experience. *Journal of Neurosurgery: Pediatrics* 20, 583–590. doi:10.3171/2017.6.PEDS1711.

Rourke, B. P. (1995). *Syndrome of nonverbal learning disabilities*. Guilford Press.

Rourke, B. P., Del Dotto, J. E., Rourke, S. B., and Casey, J. E. (1990). Nonverbal learning disabilities: The syndrome and a case study. *Journal of School Psychology* 28, 361–385. doi:10.1016/0022-4405(90)90026-4.

Rubin, R. C., and Hochwald, G. M. (1983). “Reconstitution of Cerebral Cortical Mantle following Hydrocephalus,” in *Neurobiology of Cerebrospinal Fluid 2*, ed. J. H. Wood (Boston, MA: Springer US), 821–833. doi:10.1007/978-1-4615-9269-3_52.

Rubin, R. C., Hochwald, G. M., Tiell, M., Epstein, F., Ghatak, N., and Wisniewski, H. (1976). Hydrocephalus: III. Reconstitution of the cerebral cortical mantle following ventricular shunting. *Surg Neurol* 5, 179–183.

Rubin, R. C., Hochwald, G., Tiell, M., Liwnicz, B., and Epstein, F. (2008). Reconstitution of the Cerebral Cortical Mantle in Shunt-corrected Hydrocephalus. *Developmental Medicine & Child Neurology* 17, 151–156. doi:10.1111/j.1469-8749.1975.tb03595.x.

Sahan, M. I., Majerus, S., Andres, M., and Fias, W. (2018). Functionally distinct contributions of parietal cortex to a numerical landmark task: An fMRI study. *Cortex*. doi:10.1016/j.cortex.2018.11.005.

Smith, S., Bannister, P. R., Beckmann, C., Brady, M., Clare, S., Flitney, D., et al. (2001). FSL: New tools for functional and structural brain image analysis. *NeuroImage* 13, 249–249. doi:10.1016/S1053-8119(01)91592-7.

Smith, S. M. (2002). Fast robust automated brain extraction. *Hum Brain Mapp* 17, 143–155. doi:10.1002/hbm.10062.

Smith, S. M., Fox, P. T., Miller, K. L., Glahn, D. C., Fox, P. M., Mackay, C. E., et al. (2009). Correspondence of the brain's functional architecture during activation and rest. *Proceedings of the National Academy of Sciences* 106, 13040–13045. doi:10.1073/pnas.0905267106.

Smyser, C. D., Snyder, A. Z., Shimony, J. S., Blazey, T. M., Inder, T. E., and Neil, J. J. (2013). Effects of White Matter Injury on Resting State fMRI Measures in Prematurely Born Infants. *PLOS ONE* 8, e68098. doi:10.1371/journal.pone.0068098.

Syeda, M. M., and Climie, E. A. (2014). Test Review: Wechsler Preschool and Primary Scale of Intelligence–Fourth Edition. *Journal of Psychoeducational Assessment* 32, 265–272. doi:10.1177/0734282913508620.

The MNI <-> Talairach Tool *bisweb-manual*. Available at: https://bioimagesuiteweb.github.io/bisweb-manual/tools/mni2tal.html [Accessed July 9, 2019].

Thompson, D. K., Warfield, S. K., Carlin, J. B., Pavlovic, M., Wang, H. X., Bear, M., et al. (2007). Perinatal risk factors altering regional brain structure in the preterm infant. *Brain* 130, 667–677. doi:10.1093/brain/awl277.

Thompson, G. J. (2018). Neural and metabolic basis of dynamic resting state fMRI. *NeuroImage* 180, 448–462. doi:10.1016/j.neuroimage.2017.09.010.

Tully, H. M., and Dobyns, W. B. (2014). Infantile hydrocephalus: a review of epidemiology, classification and causes. *Eur J Med Genet* 57, 359–368. doi:10.1016/j.ejmg.2014.06.002.

Turner, B. O., Paul, E. J., Miller, M. B., and Barbey, A. K. (2018). Small sample sizes reduce the replicability of task-based fMRI studies. *Communications Biology* 1, 1–10.

Ulmer, S. (2013). "Introduction," in *fMRI: Basics and Clinical Applications*, eds. S. Ulmer and O. Jansen (Berlin, Heidelberg: Springer Berlin Heidelberg), 3–5. doi:10.1007/978-3-642-34342-1_1.

Venkataramana, N. K., and Mukundan, C. R. (2011a). Evaluation of functional outcomes in congenital hydrocephalus. *J Pediatr Neurosci* 6, 4–12. doi:10.4103/1817-1745.84399.

Venkataramana, N. K., and Mukundan, C. R. (2011b). Evaluation of functional outcomes in congenital hydrocephalus. *J Pediatr Neurosci* 6, 4–12. doi:10.4103/1817-1745.84399.

WISC-V San Antonio, Tex.: NCS Pearson, Inc. : PsychCorp.

Woo, C.-W., Krishnan, A., and Wager, T. D. (2014a). Cluster-extent based thresholding in fMRI analyses: Pitfalls and recommendations. *Neuroimage* 91, 412–419. doi:10.1016/j.neuroimage.2013.12.058.

Woo, C.-W., Krishnan, A., and Wager, T. D. (2014b). Cluster-extent based thresholding in fMRI analyses: Pitfalls and recommendations. *NeuroImage* 91, 412–419. doi:10.1016/j.neuroimage.2013.12.058.

Woolrich, M. W., Behrens, T. E. J., Beckmann, C. F., Jenkinson, M., and Smith, S. M. (2004). Multilevel linear modelling for FMRI group analysis using Bayesian inference. *NeuroImage* 21, 1732–1747. doi:10.1016/j.neuroimage.2003.12.023.

Woolrich, M. W., Ripley, B. D., Brady, M., and Smith, S. M. (2001). Temporal Autocorrelation in Univariate Linear Modeling of FMRI Data. *NeuroImage* 14, 1370–1386. doi:10.1006/nimg.2001.0931.

Worsley, K. J., Liao, C. H., Aston, J., Petre, V., Duncan, G. H., Morales, F., et al. (2002). A General Statistical Analysis for fMRI Data. *NeuroImage* 15, 1–15. doi:10.1006/nimg.2001.0933.

WPPSI-IV *South County Child & Family Consultants*. Available at: https://southcountychildandfamily.com/wppsi-iv/ [Accessed April 11, 2019].

Wright, Z., Larrew, T. W., and Eskandari, R. (2016). Pediatric Hydrocephalus: Current State of Diagnosis and Treatment. *Pediatrics in Review* 37, 478–490. doi:10.1542/pir.2015-0134.

Yadav, Y. R., Parihar, V., Pande, S., Namdev, H., and Agarwal, M. (2012). Endoscopic third ventriculostomy. *J Neurosci Rural Pract* 3, 163–173. doi:10.4103/0976-3147.98222.

Yale Journal of Sociology | Sociology Available at: https://sociology.yale.edu/publications/yale-journal-sociology [Accessed August 6, 2019].

Yeates, K. O., Loss, N., Colvin, A. N., and Enrile, B. G. (2003). Do children with myelomeningocele and hydrocephalus display nonverbal learning disabilities? An empirical approach to classification. *Journal of the International Neuropsychological Society* 9, 653–662. doi:10.1017/S1355617703940057.

Yuan, W., Holland, S. K., Shimony, J. S., Altaye, M., Mangano, F. T., Limbrick, D. D., et al. (2015). Abnormal structural connectivity in the brain networks of children with hydrocephalus. *Neuroimage Clin* 8, 483–492. doi:10.1016/j.nicl.2015.04.015.

Yuan, W., Meller, A., Shimony, J. S., Nash, T., Jones, B. V., Holland, S. K., et al. (2016). Left hemisphere structural connectivity abnormality in pediatric hydrocephalus patients following surgery. *Neuroimage Clin* 12, 631–639. doi:10.1016/j.nicl.2016.09.003.

Zahl, S. M., Egge, A., Helseth, E., Skarbø, A.-B., and Wester, K. (2019). Quality of life and physician-reported developmental, cognitive, and social problems in children with benign

external hydrocephalus—long-term follow-up. *Childs Nerv Syst* 35, 245–250. doi:10.1007/s00381-018-4016-2.

Zhang, S., Li, X., Lv, J., Jiang, X., Guo, L., and Liu, T. (2016). Characterizing and Differentiating Task-based and Resting State FMRI Signals via Two-stage Sparse Representations. *Brain Imaging Behav* 10, 21–32. doi:10.1007/s11682-015-9359-7.

Appendix

Appendix A – MRI CFMM Protocol

\\USER\DeRibaupierre\BV_IVH\2018\MPRAGE sag 32ch_1mmIso
TA: 4:42 PM: FIX Voxel size: 1.0×1.0×1.0 mmPAT: 3 Rel. SNR: 1.00 : tfl

Properties

Prio recon	Off
Load images to viewer	On
Inline movie	Off
Auto store images	On
Load images to stamp segments	On
Load images to graphic segments	Off
Auto open inline display	Off
Auto close inline display	Off
Start measurement without further preparation	Off
Wait for user to start	On
Start measurements	Single measurement

Routine

Slab group	1
Slabs	1
Dist. factor	50 %
Position	R8.1 A10.6 F24.8 mm
Orientation	Sagittal
Phase enc. dir.	A >> P
AutoAlign	---
Phase oversampling	0 %
Slice oversampling	0.0 %
Slices per slab	160
FoV read	256 mm
FoV phase	93.8 %
Slice thickness	1.00 mm
TR	2300.0 ms
TE	2.93 ms
Averages	1
Concatenations	1
Filter	Prescan Normalize, Elliptical filter
Coil elements	HEA;HEP

Contrast - Common

TR	2300.0 ms
TE	2.93 ms
Magn. preparation	Non-sel. IR
TI	900 ms
Flip angle	9 deg
Fat suppr.	None
Water suppr.	None

Contrast - Dynamic

Averages	1
Averaging mode	Long term
Reconstruction	Magnitude
Measurements	1
Multiple series	Off

Resolution - Common

FoV read	256 mm
FoV phase	93.8 %
Slice thickness	1.00 mm
Base resolution	256
Phase resolution	100 %
Slice resolution	100 %
Phase partial Fourier	Off
Slice partial Fourier	Off

Resolution - Common

Interpolation	Off

Resolution - iPAT

PAT mode	GRAPPA
Accel. factor PE	3
Ref. lines PE	64
Accel. factor 3D	1
Reference scan mode	Integrated

Resolution - Filter Image

Image Filter	Off
Distortion Corr.	Off
Prescan Normalize	On
Unfiltered images	Off
Normalize	Off
B1 filter	Off

Resolution - Filter Rawdata

Raw filter	Off
Elliptical filter	On

Geometry - Common

Slab group	1
Slabs	1
Dist. factor	50 %
Position	R8.1 A10.6 F24.8 mm
Orientation	Sagittal
Phase enc. dir.	A >> P
Slice oversampling	0.0 %
Slices per slab	160
FoV read	256 mm
FoV phase	93.8 %
Slice thickness	1.00 mm
TR	2300.0 ms
Multi-slice mode	Single shot
Series	Interleaved
Concatenations	1

Geometry - AutoAlign

Slab group	1
Position	R8.1 A10.6 F24.8 mm
Orientation	Sagittal
Phase enc. dir.	A >> P
AutoAlign	---
Initial Position	R8.1 A10.6 F24.8
R	8.1 mm
A	10.6 mm
F	24.8 mm
Initial Rotation	0.00 deg
Initial Orientation	Sagittal

Geometry - Navigator

Geometry - Tim Planning Suite

Set-n-Go Protocol	Off
Table position	H
Table position	0 mm
Inline Composing	Off

System - Miscellaneous

Positioning mode	FIX
Table position	H
Table position	0 mm
MSMA	S - C - T
Sagittal	R >> L
Coronal	A >> P
Transversal	F >> H
Coil Combine Mode	Sum of Squares
Save uncombined	Off
Matrix Optimization	Off
AutoAlign	---
Coil Select Mode	Default

System - Adjustments

B0 Shim mode	Standard
B1 Shim mode	TrueForm
Adjust with body coil	Off
Confirm freq. adjustment	Off
Assume Dominant Fat	Off
Assume Silicone	Off
Adjustment Tolerance	Auto

System - Adjust Volume

Position	R8.1 A10.6 F24.8 mm
Orientation	Sagittal
Rotation	0.00 deg
A >> P	240 mm
F >> H	256 mm
R >> L	160 mm
Reset	Off

System - pTx Volumes

B1 Shim mode	TrueForm
Excitation	Non-sel.

System - Tx/Rx

Frequency 1H	123.210901 MHz
Correction factor	1
Gain	Low
Img. Scale Cor.	1.000
Reset	Off
? Ref. amplitude 1H	0.000 V

Physio - Signal1

1st Signal/Mode	None
TR	2300.0 ms
Concatenations	1

Physio - Cardiac

Magn. preparation	Non-sel. IR
TI	900 ms
Fat suppr.	None
Dark blood	Off
FoV read	256 mm
FoV phase	93.8 %
Phase resolution	100 %

Physio - PACE

Resp. control	Off
Concatenations	1

Inline - Common

Subtract	Off

Inline - Common

Measurements	1
StdDev	Off
Save original images	On

Inline - MIP

MIP-Sag	Off
MIP-Cor	Off
MIP-Tra	Off
MIP-Time	Off
Save original images	On

Inline - Composing

Inline Composing	Off
Distortion Corr.	Off

Inline - MapIt

Save original images	On
MapIt	None
Flip angle	9 deg
Measurements	1
TR	2300.0 ms
TE	2.93 ms

Sequence - Part 1

Introduction	On
Dimension	3D
Elliptical scanning	Off
Reordering	Linear
Asymmetric echo	Off
Flow comp.	No
Multi-slice mode	Single shot
Echo spacing	6.6 ms
Bandwidth	240 Hz/Px

Sequence - Part 2

RF pulse type	Fast
Gradient mode	Performance
Excitation	Non-sel.
RF spoiling	On
Incr. Gradient spoiling	Off
Turbo factor	160

Sequence - Assistant

Mode	Off

\\USER\DeRibaupierre\BV_IVH\2018\ep_bold_mb4_comparison

TA: 10:08 PM: FIX Voxel size: 2.5×2.5×2.5 mmPAT: Off Rel. SNR: 1.00 : epfid

Properties

Prio recon	Off
Load images to viewer	On
Inline movie	Off
Auto store images	On
Load images to stamp segments	Off
Load images to graphic segments	Off
Auto open inline display	Off
Auto close inline display	Off
Start measurement without further preparation	Off
Wait for user to start	On
Start measurements	Single measurement

Routine

Slice group	1
Slices	48
Dist. factor	0 %
Position	R1.4 A8.1 F13.6 mm
Orientation	T > C-20.8
Phase enc. dir.	A >> P
AutoAlign	---
Phase oversampling	0 %
FoV read	208 mm
FoV phase	100.0 %
Slice thickness	2.50 mm
TR	1000 ms
TE	30.00 ms
Multi-band accel. factor	4
Filter	Prescan Normalize
Coil elements	HEA;HEP

Contrast - Common

TR	1000 ms
TE	30.00 ms
MTC	Off
Magn. preparation	None
Flip angle	40 deg
Fat suppr.	Fat sat.

Contrast - Dynamic

Averaging mode	Long term
Reconstruction	Magnitude
Measurements	600
Delay in TR	0 ms
Multiple series	Off

Resolution - Common

FoV read	208 mm
FoV phase	100.0 %
Slice thickness	2.50 mm
Base resolution	84
Phase resolution	100 %
Phase partial Fourier	7/8
Interpolation	Off

Resolution - iPAT

PAT mode	None

Resolution - Filter Image

Distortion Corr.	Off

Resolution - Filter Image

Prescan Normalize	On

Resolution - Filter Rawdata

Raw filter	Off
Elliptical filter	Off
Hamming	Off

Geometry - Common

Slice group	1
Slices	48
Dist. factor	0 %
Position	R1.4 A8.1 F13.6 mm
Orientation	T > C-20.8
Phase enc. dir.	A >> P
FoV read	208 mm
FoV phase	100.0 %
Slice thickness	2.50 mm
TR	1000 ms
Multi-slice mode	Interleaved
Series	Interleaved
Multi-band accel. factor	4

Geometry - AutoAlign

Slice group	1
Position	R1.4 A8.1 F13.6 mm
Orientation	T > C-20.8
Phase enc. dir.	A >> P
AutoAlign	---
Initial Position	R1.4 A8.1 F13.6
R	1.4 mm
A	8.1 mm
F	13.6 mm
Initial Rotation	0.00 deg
Initial Orientation	T > C
T > C	-20.8
> S	0.0

Geometry - Saturation

Fat suppr.	Fat sat.
Special sat.	None

Geometry - Tim Planning Suite

Set-n-Go Protocol	Off
Table position	H
Table position	0 mm
Inline Composing	Off

System - Miscellaneous

Positioning mode	FIX
Table position	H
Table position	0 mm
MSMA	S - C - T
Sagittal	R >> L
Coronal	A >> P
Transversal	F >> H
Coil Combine Mode	Sum of Squares
Matrix Optimization	Off
AutoAlign	---
Coil Select Mode	On - AutoCoilSelect

System - Adjustments

B0 Shim mode	Brain
B1 Shim mode	TrueForm
Adjust with body coil	Off
Confirm freq. adjustment	Off
Assume Dominant Fat	Off
Assume Silicone	Off
Adjustment Tolerance	Auto

System - Adjust Volume

Position	R1.4 A8.1 F13.6 mm
Orientation	T > C-20.8
Rotation	0.00 deg
A >> P	208 mm
R >> L	208 mm
F >> H	120 mm
Reset	Off

System - pTx Volumes

B1 Shim mode	TrueForm
Excitation	Standard

System - Tx/Rx

Frequency 1H	123.210901 MHz
Correction factor	1
Gain	High
Img. Scale Cor.	1.000
Reset	Off
? Ref. amplitude 1H	0.000 V

Physio - Signal1

1st Signal/Mode	None
TR	1000 ms
Multi-band accel. factor	4

BOLD

GLM Statistics	Off
Dynamic t-maps	Off
Ignore meas. at start	0
Ignore after transition	0
Model transition states	On
Temp. highpass filter	On
Threshold	4.00
Paradigm size	20
Meas[1]	Baseline
Meas[2]	Baseline
Meas[3]	Baseline
Meas[4]	Baseline
Meas[5]	Baseline
Meas[6]	Baseline
Meas[7]	Baseline
Meas[8]	Baseline
Meas[9]	Baseline
Meas[10]	Baseline
Meas[11]	Active
Meas[12]	Active
Meas[13]	Active
Meas[14]	Active
Meas[15]	Active
Meas[16]	Active
Meas[17]	Active
Meas[18]	Active
Meas[19]	Active
Meas[20]	Active
Motion correction	Off

BOLD

Spatial filter	Off
Measurements	600
Delay in TR	0 ms
Multiple series	Off

Sequence - Part 1

Introduction	Off
Contrasts	1
Flow comp.	No
Multi-slice mode	Interleaved
Free echo spacing	Off
Echo spacing	0.6 ms
Bandwidth	2126 Hz/Px

Sequence - Part 2

EPI factor	84
Gradient mode	Performance
Excitation	Standard
RF spoiling	Off

Sequence - Special

Excite pulse duration	2560 us
Single-band images	Off
MB LeakBlock kernel	Off
MB dual kernel	Off
MB RF phase scramble	Off
SENSE1 coil combine	Off
Invert RO/PE polarity	Off
PF omits higher k-space	Off
Disable freq. update	Off
Force equal slice timing	Off
Online multi-band recon.	Online
FFT scale factor	1.00
Physio recording	Off
Triggering scheme	Standard

Appendix B – Permission to use Dartmouth Database of Children's Faces

---

From: Kirsten Dalrymple[redacted]
Sent: June 4, 2019 10:46 AM
To: Ikhlas Ahmed Hashi
Cc: Sandrine De Ribaupierre; Estelle Ansermet
Subject: Re: Permission to Use Copyrighted Material in a Doctoral/Master's Thesis

Hi Ikhlas,

Congratulations on finishing your thesis! The parent of this model from the Dartmouth Database of Children's Faces has given permission for her image to be used for publication, so you are permitted to publish it as part of your thesis.

All the best,
Kirsten

Kirsten Dalrymple, PhD
Research Associate & Lecturer I Institute of Child Development I [redacted]
University of Minnesota I[redacted]

Appendix C – Research Ethics Board Approval Notice

Western Research

Date: 4 April 2019

To: Sandrine de Ribaupierre

Project ID: 104107

Study Title: Brain variability in children with previous IVH - a pilot study

Application Type: HSREB Amendment Form

Review Type: Delegated

Full Board Reporting Date: April 23,2019

Date Approval Issued: 04/Apr/2019

REB Approval Expiry Date: 30/Jan/2020

Dear Sandrine de Ribaupierre ,

The Western University Health Sciences Research Ethics Board (HSREB) has reviewed and approved the WREM application form for the amendment, as of the date noted above.

Documents Approved:

Document Name	Document Type	Document Date
104107protocol_Changes_April2019	Protocol	Received April 1, 2019
BRIEF2	Paper Survey	Received April 1, 2019
Brochure_hydrocephalus	Recruitment Materials	Received April 1, 2019
Email_phone_Script	Recruitment Materials	Received April 1, 2019
poster_hydrocephalus	Recruitment Materials	Received April 1, 2019
REB_Brain_Variability_IVH_LOC_control_April	Consent Form	01/Apr/2019
REB_Brain_Variability_IVH_LOC_patient_April	Consent Form	01/Apr/2019
SES	Online Survey	Received April 1, 2019
SES	Paper Survey	Received April 1, 2019

REB members involved in the research project do not participate in the review, discussion or decision.

The Western University HSREB operates in compliance with, and is constituted in accordance with, the requirements of the TriCouncil Policy Statement: Ethical Conduct for Research Involving Humans (TCPS 2); the International Conference on Harmonisation Good Clinical Practice Consolidated Guideline (ICH GCP); Part C, Division 5 of the Food and Drug Regulations; Part 4 of the Natural Health Products Regulations; Part 3 of the Medical Devices Regulations and the provisions of the Ontario Personal Health Information Protection Act (PHIPA 2004) and its applicable regulations. The HSREB is registered with the U.S. Department of Health & Human Services under the IRB registration number IRB 00000940.

Please do not hesitate to contact us if you have any questions.

Sincerely,

Karen Gopaul, Ethics Officer on behalf of Dr. Philip Jones, HSREB Vice-Chair

[redacted]

Curriculum Vitae

Name:	Ikhlas Ahmed Hashi
Post-secondary Education and Degrees:	University of Western Ontario London, Ontario, Canada 2012-2017 BSc Major in Medical Science Minor in Medical Cell Biology University of Western Ontario London, Ontario, Canada 2017-2019 MSc Neuroscience
Honours and Awards:	Western Scholarship of Excellence University of Western Ontario 2012-2013 Dean's Honor List University of Western Ontario 2012-2013, 2014-2015
Related Work Experience:	Graduate Research Assistant University of Western Ontario 2017-2019

Publications and Conference Presentations:

Hashi, I., Ansermet, E., de Ribaupierre, S., & Eagleson, R. *Changes in resting state connectivity in children with infantile hydrocephalus*. (2018, September). Abstract accepted to the Sixth Biennial Conference on Brain Connectivity, Montreal, QC.

Hashi, I, A., de Ribaupierre, S., & Eagleson, R. (2019, May). *Neurodevelopmental outcomes in infantile hydrocephalus: an fMRI case study*. Abstract accepted to the Southern Ontario Neuroscience Association Annual Meeting, Windsor, ON.

Ghahari, D., **Hashi, I, A.,** Morton, J, B., de Ribaupierre, S., & Eagleson, R., (2019, May). *Executive dysfunction and white matter integrity in children with hydrocephalus years after surgery*. Abstract accepted to the Southern Ontario Neuroscience Association Annual Meeting, Windsor, ON.

Hashi, I., Ansermet, E., Eagleson, R., & de Ribaupierre, S., (2019, May). *Changes in resting state neuronal networks and non-verbal learning in children with previous infantile hydrocephalus.* Abstract accepted to the Thirteenth Annual Canadian Neuroscience Meeting, Toronto, ON.

Hashi, I, A., de Ribaupierre, S., & Eagleson, R., (2019, May). *Neurodevelopmental outcomes in infantile hydrocephalus: an fMRI case study.* Abstract accepted to the Fourth annual Dr. Benjamin Goldberg Developmental Disabilities Research Day, London, ON.

Hashi, I, A., de Ribaupierre, S., & Eagleson, R., (2019, May). *Neurodevelopmental outcomes in infantile hydrocephalus: an fMRI case study.* Abstract accepted to the Child Health Research Day 2019, London, ON.

Hashi, I., Ansermet, E., Eagleson, R., & de Ribaupierre, S., (2019, June). *Effects of infantile hydrocephalus on functional connectivity of resting state networks.* Abstract accepted to the Annual Meeting of the Organization for Human Brain Mapping, Rome, Italy.

Memberships:

Canadian Association of Neuroscience
Student Member
2018-2019

Southern Ontario Neuroscience Association
Student Member
2019